FUNDAMENTAL STUDIES ON ULTRASONIC CAVITATION-ASSISTED MOLTEN METAL PROCESSING OF A356-NANOCOMPOSITES

by

XIAODA LIU

LAURENTIU NASTAC, COMMITTEE CHAIR

NAGY EL-KADDAH
MARK WEAVER
BRIAN JORDON

A THESIS

Submitted in partial fulfillment of the requirements
for the degree of Master of Science in the
Department of Metallurgical and Materials Engineering
in the Graduate School of
The University of Alabama

TUSCALOOSA, ALABAMA

2013

ABSTRACT

The usage of lightweight high-performance components is expected to increase significantly as automotive, military and aerospace industries are required to improve the energy efficiency and the performance of their products. A356, which is much lighter than steel, is an attractive replacement material. Therefore, it is of great interest to enhance its properties. There is strong evidence that the microstructure and mechanical properties can be considerably improved if nanoparticles are used as reinforcement to form metal-matrix-nano-composite (MMNC). Several recent studies revealed that ultrasonic vibration is highly efficient in dispersing nanoparticles into the melt and producing MMNC.

In this thesis, a detailed analysis of the microstructure and mechanical properties is provided for an A356 alloy enhanced with Al_2O_3 and SiC nanoparticles via ultrasonic processing. Each type of the nanoparticles was inserted into the A356 molten metal and dispersed by ultrasonic cavitation and acoustic streaming technology (UST) to avoid agglomeration or coalescence. The results showed that microstructures were greatly refined and with the addition of nanoparticles, tensile strength, yield strength and elongation increased significantly. SEM and EDS analyses were also performed to analyze the dispersion of nanoparticles in the A356 matrix. Since the ultrasonic energy is concentrated in a small region under the ultrasonic probe, it is difficult to ensure proper cavitation and acoustic streaming for efficient dispersion of the nanoparticles (especially in larger UST systems) without to determine the suitable ultrasonic parameters via modeling and simulation. Accordingly, another goal of this thesis was to develop well-

controlled UST experiments that can be used in the development and validation of a recently developed UST modeling and simulation tool.

LIST OF ABBREVIATIONS AND SYMBOLS

UST	Ultrasonic technology
DTA	Differential thermal analysis
SEM	Scanning Electron Microscopy
EDS	Energy dispersive X-ray spectroscopy
CFD	Computational fluid dynamics
SDAS	Secondary Dendrite Arm Spacing
ρ	Density
I(t)	Nucleation rate

ACKNOWLEDGMENTS

I am pleased to have this opportunity to thank the colleagues, friends, and faculty members who have helped me with this research project. I am most indebted to Dr. Laurentiu Nastac, my advisor and the chairman of this dissertation, for sharing his research expertise and wisdom, as well as his patient supervision on the project. I would also like to thank all of my committee members, Dr. Nagy El-Kaddah, Dr. Mark Weaver, and Dr. Brian Jordon, for their valuable input, inspiring questions, and support of both the thesis and my academic progress. A special thanks to my colleagues Shian Jia and Akash Patel who helped me run the system countless times and worked long hours including weekends to help along the way. I would also like to thank Bob Fanning for his assistance in my experiments.

Finally, this research would not have been possible without the support of my friends and fellow graduate students and of course of my family who have never stopped encouraging me to persist in my research endeavor.

CONTENTS

Page

LIST OF TABLES

Page

LIST OF FIGURES

Page

1.0 INTRODUCTION

Aluminum matrix composites have the potential to offer desirable properties, including low density, high specific strength, high specific stiffness, excellent wear resistance and controllable expansion coefficient, which make them attractive for numerous applications in aerospace, automobile, and military industries [70-73].

During fabrication of the cast composites, it has been found that larger dendritic structures which are present during solidification may lead to particle clustering, whereas fine dendrite or regular globular ones may produce a more uniform distribution of the particles [74,75]. Hence, any processing step that can make grain size smaller can reduce the heterogeneity of the reinforcement distribution in the solidified region, which in turn will improve the mechanical properties of the aluminum matrix composites components. Also, according to Hall-Petch strengthening theory, the smaller the grain sizes the harder the material.

Generally, micro-ceramic particles are used to improve the yield and ultimate strength (UTS) of the metal. It is of interest to use nano-sized ceramic particles to strengthen metal matrix nano-composite (MMNC), while maintaining good ductility [76, 77]. Currently, there are several fabrication methods of MMNCs, including mechanical alloying with high energy milling [78], ball milling [79], nano-sintering [80], vortex process [76], spray deposition, electrical plating, sol-gel synthesis, laser deposition, etc. The mixing of nano-sized ceramic particles is lengthy, expensive, and energy consuming. The solid-state technologies discussed above that are used for manufacturing of Al MMCs suffer from size and complexity limitations of the components. The liquid-state technologies including stir-casting and compo-casting are attractive due to their low

cost, high yield, and near net shaping capability. However, the stir casting process cannot disperse the nanoparticles uniformly into the melt due to their large surface-to-volume ratio and poor wettability.

Several recent studies revealed that ultrasonic vibration is highly efficient in dispersing nanoparticles into the melt [34, 40]. Ultrasonic vibration has been extensively used in (I) purifying, degassing, and refinement of metallic melt [38-40]; and (II) for introducing the ultrasonic energy into a liquid that will induce nonlinear effects such as cavitation and acoustic streaming. Ultrasonic cavitation can create small-size transient domains that could reach very high temperatures and pressures as well as extremely high heating and cooling rates. The shock force occurring during ultrasonic cavitation coupled with local high temperatures could break nanoparticle clusters and clean the surface of the particles [48-50]. Furthermore, ultrasonic vibration can improve the wettability between the reinforced nanoparticles and the metal matrix, and distribute particles uniformly into the metal matrix.

Among various types of ceramic particles such as oxides, nitrides, or carbides, Al_2O_3 and SiC are widely used as reinforcement particles due to their relatively good thermal and chemical stability as compared to other types of reinforcements [9, 10]. In this article, the effects of the ultrasonically dispersed Al_2O_3 and SiC nanoparticles on the as-cast microstructure are studied.

The purpose of this work is to perform a fundamental research on Al_2O_3 and SiC nanoparticles reinforced A356 nanocomposites fabricated by ultrasonic method. The goals are as follows:

(i) Apply ultrasonic cavitation and acoustic streaming for proper dispersion of the nanoparticles into the molten metal. A356 alloy will be used as the matrix alloy.

Al_2O_3 nanoparticles with an average diameter of 20nm and SiC nanoparticles with an average diameter of 50 nm will be used as the reinforcement materials.

(ii) Study the dispersion of nanoparticles in the A356 nanocomposites under SEM (Scanning Electron Microscopy).

(iii) Investigate the effects of the main ultrasonic and solidification process parameters on the microstructures and mechanical properties of the A356 nanocomposite material.

(iv) Develop well-controlled UST experiments that will be used in the development and validation of the UST dispersion modeling and simulation tool currently under development at the University of Alabama.

The thesis is presented in the following sequence: chapter II provides a literature review, chapter III will present the experimental approach, chapter IV will present and discuss in detail the experimental results and chapter V will present the conclusions and recommended future work.

2.0 LITERATURE REVIEW

The term "Metal Matrix Nano-Composites (MMNCs)" broadly refers to a composite system that is based on metal or alloy substrate, combined with metallic or non-metallic nano-scale reinforcements. There is strong evidence that mechanical properties of a cast component can be considerably improved if nanoparticles are used as a reinforcement to form a metal-matrix-nano-composite (MMNC).

2.1 A356 ALUMINUM ALLOY

Aluminum-silicon (Al-Si) alloys compromise 85 to 90 percent of the total Al casting parts produced commercially, and are used extensively in industry due to their superior properties, including good corrosion resistance, low coefficient of thermal expansion, excellent castability, low density, high strength-to-weight ratio, and improved mechanical properties over a wide range of temperatures [1]. In particular, alloy A356 is a 7 wt. %Si-0.3wt. % Mg alloy with 0.2 wt. % Fe (max) and 0.10 wt. % Zn (max). Alloy A356 has greater elongation, higher strength and considerably higher ductility than Alloy 356. A356 has improved mechanical properties because of lower iron content, compared to 356. Typical applications are airframe castings, machine parts, truck chassis parts, aircraft and missile components, and structural parts requiring high strength [2]. Even though A356 exhibits good performance in as-cast as well as in its heat-treated form, the alloy has several limitations.

For example, A356 exhibits moderate machinability, low stiffness, and limited strength under high temperatures, which limits its application to components subjected to extreme temperature conditions [3]. In addition, A356 exhibits low room temperature wear resistance as well as the presence of defects and oxide films [4].

Therefore, further study need to be carried out to improve the mechanical performance of A356 alloy by additional element reinforcements for the expanded applications in industry.

2.2 TYPE OF NANOPARTICLES

By scaling down the particle size from micro-meter to nano-meter, better material properties could be obtained [5]. It has been reported that with a small fraction of nano-sized reinforcements, nanocomposites could obtain comparable or even far superior mechanical properties than those of micro-size particles strengthened MMCs [6-8].

Among various types of ceramic particles such as oxides, nitrides, or carbides, Al_2O_3 and SiC are widely used as reinforcement particles due to their relatively good thermal and chemical stability as compared to other types of reinforcements [9, 10].

2.3 METAL-MATRIX-COMPOSITES

Metal Matrix Composites (MMCs) reinforced with ceramic particulate offer significant performance advantages over pure metals and alloys. MMCs tailor the best properties of the two components, such as ductility and toughness of the matrix and high modulus and strength of the reinforcements [11-23]. These prominent properties of these materials enable them to be potential for numerous applications such as automotive, aerospace and military industries [24-27].

MMCs can be divided into three categories: particle reinforced MMCs, short fiber reinforced MMCs and continuous fiber reinforced MMCs. Compared to other two types of reinforcements, the fabrication cost of particulate is low [11], which makes it more economical in many applications.

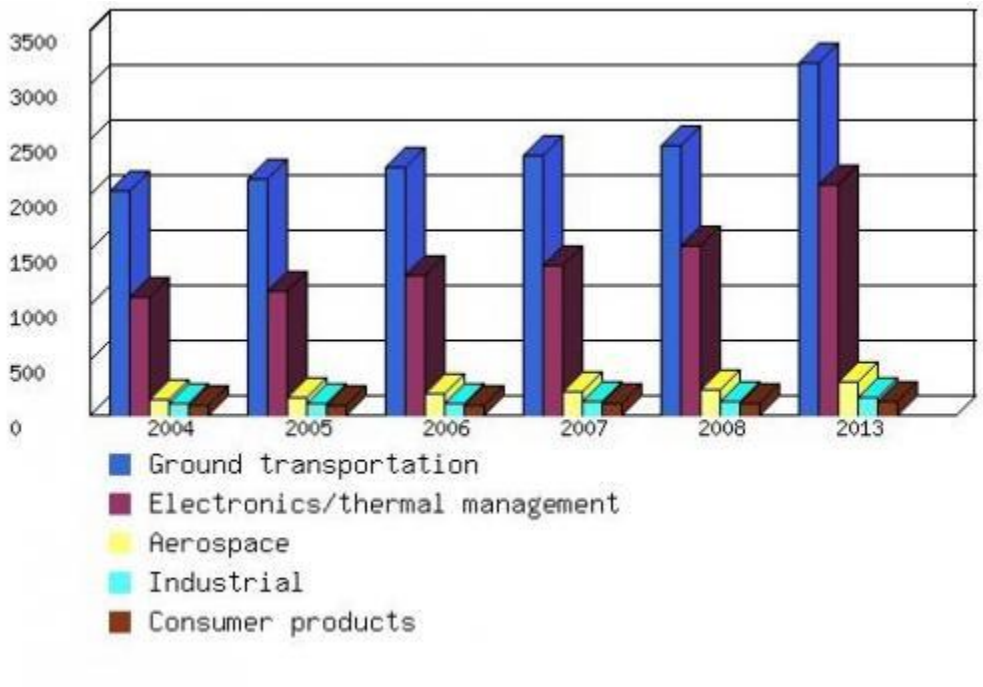

Figure 1: Global outlook of metal-matrix composites by application segment (2004-2013).

(From BCC research: http://www.bccresearch.com/)

Orowan strengthening theory could explain the strengthening mechanism of metal matrix composites [28]. The mechanism is shown schematically in Figure 2 below. According to this mechanism the yield stress is determined by the stress required for a dislocation line to pass by the two particles shown. The dislocation line is bowed around the two particles as the applied stress is increased until the dislocation line reaches a critical curvature stage 2. When this critical curvature is reached the dislocation line can then move forward without increasing its curvature (stage 3). The segments of dislocation line on either side of each particle then join, and a dislocation loop is left around each particle. As each dislocation line moves past a particle

the dislocation cell structure around the particle builds up. Hansen [23] investigated this phenomenon results in dispersion hardened metals with a high rate of strain hardening.

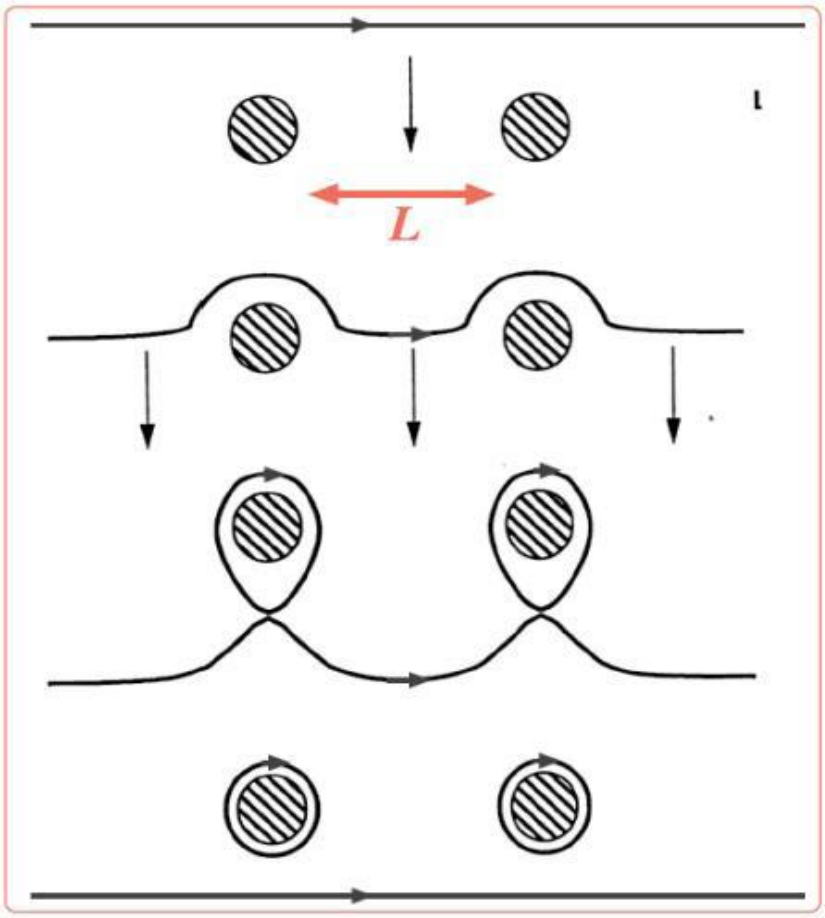

Figure 2: Orowan Strengthening Theory [23]

In many systems, Orowan strengthening is not the only mechanism at play; other mechanism such as Hall-Petch strengthening due to grain size and solute strengthening (in alloyed aluminum) also contribute to the strength of the resulting MMC. Based on the studies of strengthening

mechanism, metal matrix composites reinforced with micro-sized particles have been well investigated and applied in many fields.

A simulation of the solidification microstructure of MMCs is shown in Figure 3. The effect of the SiC reinforcement on A356 can be clealry seen in Figure 3.

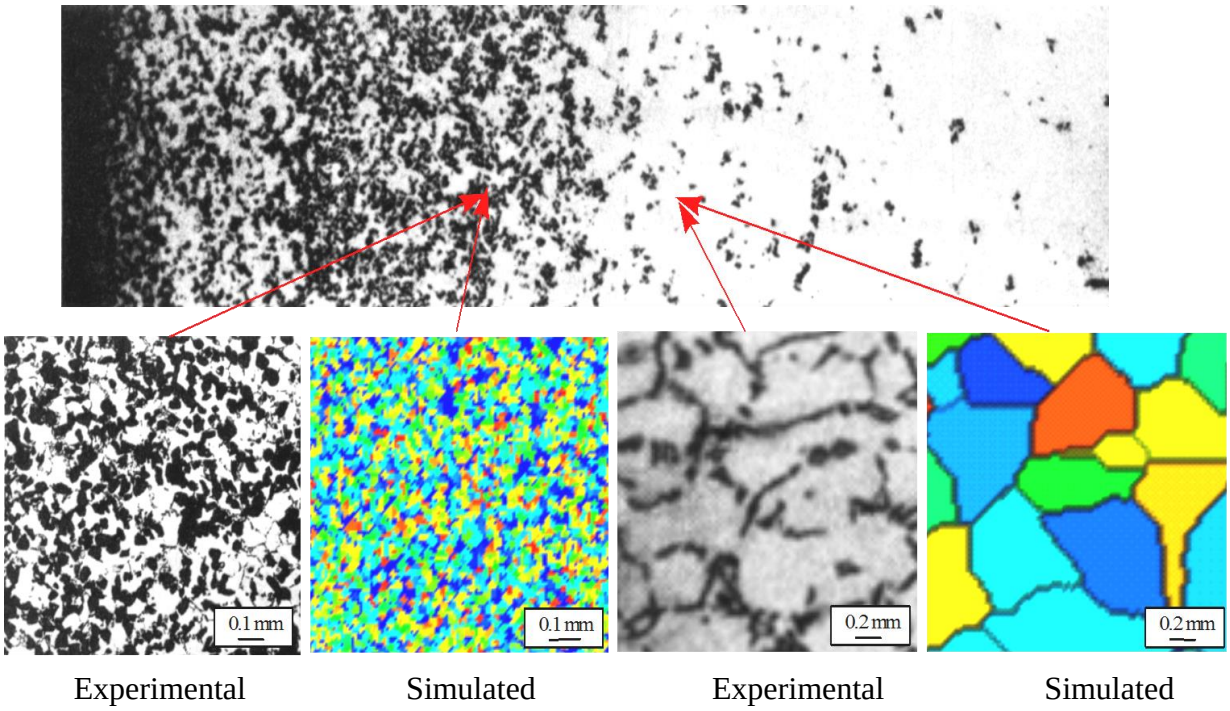

Figure 3: Simulated solidification microstructure of A356 /7 μm diameter SiC (initial particle concentration is 4.8 vol. % SiC) centrifugally-cast MMCs (centrifugal force of 100 g) [66].

2.4 FABRICATION METHODS

During fabricating of the cast composites, it has been found that larger dendritic structures which are present during solidification lead to particle clustering, whereas fine dendrite or regular globular ones produce a more uniform distribution of the particles [67,68].

Hence, from this point of view, any processing step that is capable of producing smaller grain size can reduce the heterogeneity of the reinforcement distribution in the solidified region, which in turn will improve the mechanical properties of the aluminum matrix composites (Al MMC) components.

Ultrasonic treatment of metallic alloy systems, such as Al-Si [29-32] and Al-Cu [33] alloys has been studied extensively. It has been shown that the addition of ultrasonic vibration into the melt can eliminate columnar dendritic structure, refine the equiaxed grain structure, and by casting at low superheat may also produce globular grain morphologies [29, 30].

Currently, there are several technologies for manufacturing of Al-MMCs, including mechanical alloying with high energy milling [35], vortex process [36,37], disintegrated melt deposition [38], powder metallurgy [39], ultrasonic casting [34, 40], etc. The joining of aluminum matrix composites (Al MMCs) has been studied in detail in [41-47]. During joining of Al MMCs, reinforcement particles tend to be incorporated into the molten pool once melting of base metal occurs. The solidification of such molten pool faces a problem similar to that associated with the solidification of the cast composite slurry, that is, even if uniform dispersion of particles can somehow be ensured in the melt, they can still become segregated in the inter-granular and inter-dendritic regions of the matrix due to particle pushing by the advancing solid-liquid interface during solidification [46, 47]. The particle-segregated zones in the bond region have been observed to be the sources of cracks during mechanical testing of the joint [44].

The solid-state technologies discussed above that are used for manufacturing of Al MMCs suffer from size and complexity limitations of the components. The liquid-state technologies including stir-casting and compo-casting are attractive due to their low cost, high yield, and near

net shaping capability. However, the stir casting process cannot disperse the nanoparticles uniformly into the melt due to their large surface-to-volume ratio and poor wettability.

Several recent studies revealed that ultrasonic vibration is highly efficient in dispersing nanoparticles into the melt [34, 40]. Ultrasonic vibration has been extensively used in (i) purifying, degassing, and refinement of metallic melt [38-40]; and (ii) for injecting the ultrasonic energy into a liquid that will give rise to nonlinear effects such as cavitation and acoustic streaming. Furthermore, ultrasonic vibration can improve the wettability between the reinforced nanoparticles and the metal matrix, and distribute particles uniformly into the metal matrix.

Some work has been reported that ultrasonic vibration had been used to prepare the particulate reinforced composites, and the reinforcements were added into the melts directly [48, 49]. High intensity ultrasonic waves can generate strong cavitation and acoustic streaming in the molten metal. Ultrasonic cavitation can create small-size transient domains that could reach very high temperatures and pressures as well as extremely high heating and cooling rates. The shock force occurring during ultrasonic cavitation coupled with local high temperatures could break nanoparticle clusters and clean the surface of the particles [48-50].

Fabrication Limitations of Nano-Composites:

As discussed above, different types of methods have been used to fabricate MMNCs. Other than classifying the processing routes based on the state in which the composites are fabricated, the processing routes could also be classified into ex-situ methods and in-situ methods based on the source of particles.

Ex-situ methods, which include powder metallurgy, stirring techniques, pressure infiltration and spray deposition, are usually more cost-efficient. However, the particles are easy to

agglomerate and hard to be dispersed. Reinforcements created in-situ are usually fine and well distributed, however, in-situ reinforcement have less opportunity than ex-situ ones for complex reactions involved in the in-situ fabrication routes [51].

Fabrication of MMNCs is much more complex compared to fabrication of MMCs. When the particle size scales down from the micro to the nano level, the major challenges are [51]:

1. The reaction process between the bonding interfaces is still unclear.

2. Agglomeration and clustering in bulk materials can still be observed. The dispersion during processing needs to be optimized.

3. Cost effectiveness is another factor that hinders the fabrication of nanocomposites. With the development of nanotechnology, the prices of nanofabrication should be reduced.

4. Currently, low volume and rates are obtained. A transition to high volume and high rate fabrication is pivotal to applying the technology to real industry fabrication.

5. Different processes have been applied, however modeling of these processes are needed.

2.5 AGGLOMERATION

Agglomerates of particles are usually observed in the solidified microstructure. This is due to the increase of surface area caused by the reduction of particle size, which raise the difficulty of particle introduction and homogeneous dispersion through the melt. The poor wetting between reinforcement material and the metal matrix presents a barrier to the incorporation of the dispersoid phase into the melt. The immersion of solids into liquids requires substitution of a solid-gas interface by an equivalent solid-liquid interface, and can lead to absorption or generation of energy [52,53]. The energetic of solid immersion into liquids are determined by the energy associated with the solid-gas interface, liquid gas interface and solid-liquid interface.

By definition, the surface energy ɣ is the energy required to create a unit area of new surface, and represents the extra energy possessed by the surface atoms due to the decrease in bond length between the surface atoms and interior atoms [52, 53]. When a particle is split into two smaller particles, the number of broken bonds contributes to the surface energy of each of the two particles according to Eq. (1) [52]:

$$\gamma = 0.5N\,\varepsilon\,\rho_A \qquad (1)$$

Where N is the number of the broken bonds, ε is half of the bond strength and ρ_A the number of atoms per unit area on the new surface.

Table I: Variation of surface energy with particle size (1 g of sodium chloride) [53]

Particle Size (cm)	Total Surface Area (cm^2)	Surface Energy (J/g)
0.1	28	5.6×10^{-4}
0.01	280	5.6×10^{-3}
0.001	2.8×10^{3}	5.6×10^{-2}
10^{-4} (1 µm)	2.8×10^{4}	0.56
10^{-7} (1 nm)	2.8×10^{7}	560

Changes in the size range from micron scale to nanometer, lead to great changes in physical and chemical properties of the material. In Table I it is shown the scatter of seven order of magnitude in the surface energy when the nanometer scale is reached. The massive increase in surface energy makes particle wetting from the melt more difficult, as the surface energy of the system itself is increased [52].

2.5.1 THEORETICAL MODEL

To calculate the total attractive force of nano-particles, a simplified model was employed [57]: two nano-particles entrapped inside the aluminum melt were considered, as shown in Figure 4.

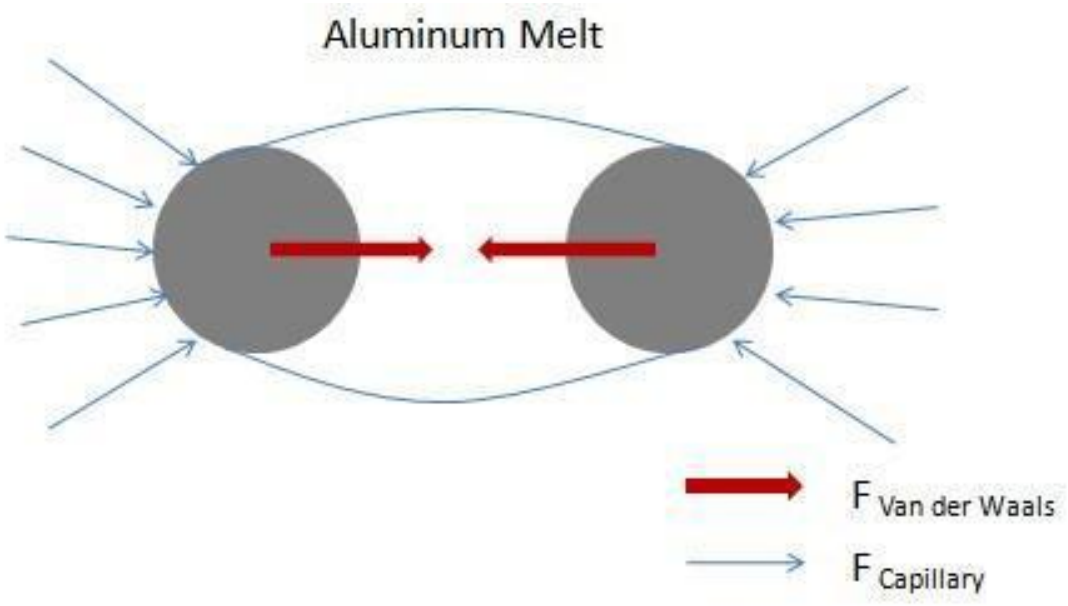

Figure 4: Model for the agglomeration of SiC nano-particles.

There are two forces that hold the two particles in the melt: (i) Van der Waals force, and (ii) capillary force applied by the melt surface tension. These two forces are independent and vary with the distance between these two particles. The maxima of these two forces are calculated separately and then added together to get the force needed to break-up particle agglomeration.

To calculate the Van der Waals force, the Lennard-Jones potential model was employed. The Lennard-Jones potential is a mathematically simple model that describes the interaction between a pair of neutral atoms or molecules. The expression of Lennard- Jones potential is

$$V(r) = 4\varepsilon[\left(\frac{\sigma}{r}\right)^{12} - \left(\frac{\sigma}{r}\right)^{6}] \quad (2)$$

Where ε is the depth of the potential well, σ is the (finite) distance at which the inter-particle potential is zero, and r is the distance between the particles.

The potential energy of the two particles is obtained vs. the distance between them, and the derivative of the potential is calculated to obtain the force between these two particles.

$$Potential = \int_{V1} dV_1 \int_{V2} q^2 V(r) dV_2 \quad (3)$$

Where dV_1 and dV_2 are the infinitesimal volume elements in the particles of volume V_1 and V_2, respectively. As shown in Figure 5, r is the distance between the volume elements dV_1 and dV_2, q is the molecule density and V(r) is the Lennard-Jones potential model.

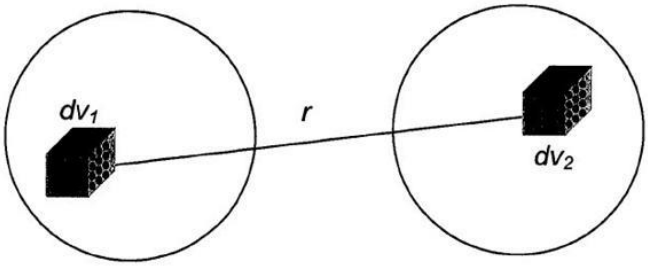

Figure 5: Schematic representation of the interaction force between two particles.

Eq. (1) was numerically integrated and the Van der Waals force was calculated as the derivative of potential and plotted, as shown in Figure 6, where attractive forces are denoted as positive values and the repulsive forces shown as negative values. As the radius of the nano-particles varies from 1 nm to 100 nm, the force increased. For the SiC nano-particles with a diameter of 50 nm, the maximum Van der Waals force is approximately 70 nN.

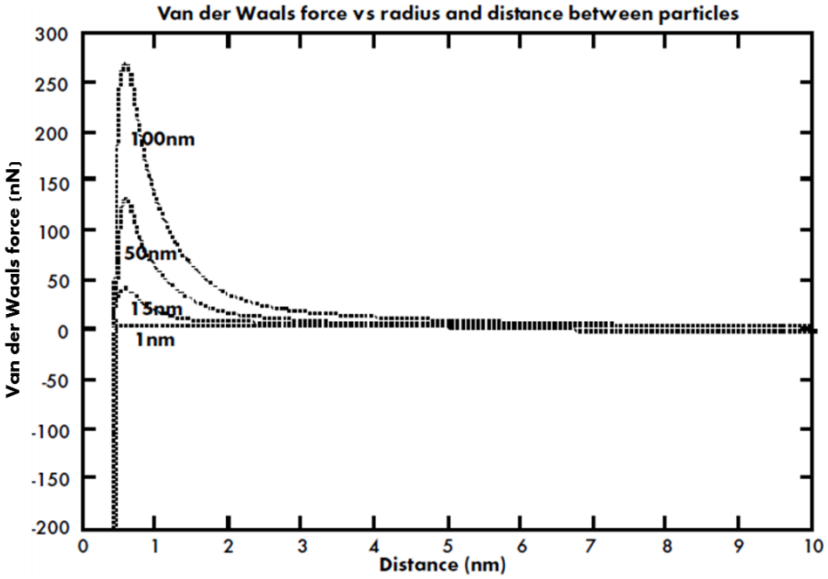

Figure 6: Van der Waals force vs. distance between SiC nano-particles [69]

To calculate the capillary force, we consider one particle sitting on top of the aluminum melt layer. Due to the poor wettability between the SiC particles and aluminum matrix, the nano-particle/melt system should be considered as hydrophobic, which means the force generated by the melt surface tends to push the particles out of the melt. This force is given by:

$$F_C = 2\pi(R \sin\theta_C)\gamma \sin(\theta_C + \alpha) \quad (4)$$

Where γ is the surface tension coefficient, θ_C is the filling angle, and α is the contact angle. The maximum capillary force is calculated to be approximately 25 nN according to this equation.

2.6 ULTRASONIC CAVITATION AND DISPERSION

Several attempts have been made to overcome the agglomeration of particles. Li. et al. [54-57] fabricated Al and Mg based nanocomposites using ultrasonic cavitation. In the ultrasonic cavitation-based solidification process, transient micro hot spot with the temperature of about 5,000 K and pressure above 1,000 atm can be formed by ultrasonic cavitation. The strong heating and cooling rates during the formation process is composed of hot spots that can break nanoparticles cluster and clean the particle surface. The schematic of ultrasonic cavitation-based solidification processing is shown in Figure 7. In the ultrasonic cavitation-based solidification processing, nanoparticles are placed on the surface of molten metal. Then the ultrasonic vibration is executed on the molten metals for a specified period of time until all the particles are distributed in the liquid metal.

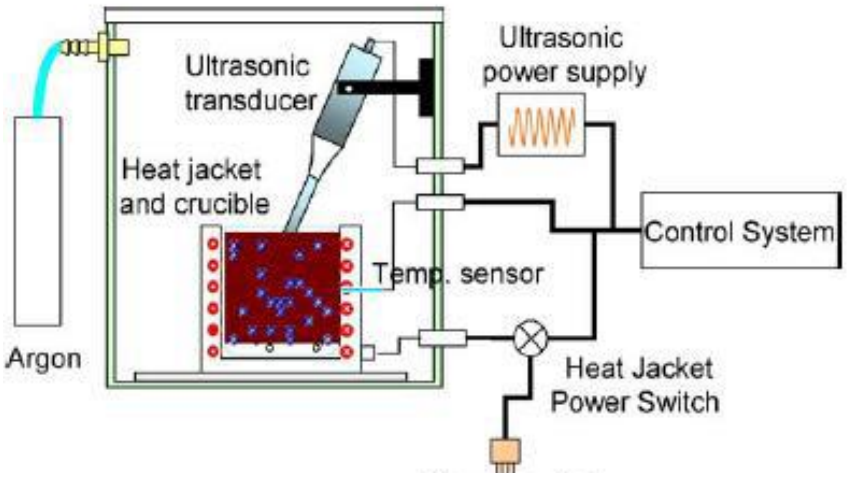

Figure 7: Schematic of experimental setup of ultrasonic method [54-57].

Yang et al. [57] fabricated bulk Al-based nanocomposites with nano-sized SiC by ultrasonic cavitation-based casting method. It is shown that the nano-sized SiC particles are dispersed well in the matrix and the yield strength of A356 alloy was improved more than 50% with only 2.0 wt.% of nano-sized SiC particles. Partial oxidation of SiC nanopartilces resulted in the formation of SiO_2 in the matrix. The study suggests that strong ultrasonic nonlinear effects could efficiently disperse nanoparticles (less than 100 nm) into alloy melts while possibly enhancing their wettability, thus making the production of as-cast high performance lightweight MMNCs feasible.

Modeling Approaches:

A fully couple energy, mass, acoustic, and compressible fluid flow models to study ultrasonic cavitation was developed by Nastac [62-63.]. In the multi-phase ultrasonic cavitation modeling approach presented in Reference [62-63], a basic two-phase cavitation model was used that consists of using the standard viscous flow equations governing the transport of phases (Eulerian multi-phase) and the turbulence model. In the cavitation region, the liquid-bubble mass transfer was shown to be governed by the cavity (bubble) transport equation:

$$\frac{\partial}{\partial t}\left(f_b\ \rho_b\right)+\nabla\cdot\left(f_b\ \rho_b\ \vec{V}_b\right)=R_G-R_C \tag{5}$$

Where *b* subscript denotes the cavitation bubble phase, f_b is the bubble volume fraction, ρ_b is the bubble density, $\vec{V}_b$ is the bubble phase velocity, R_G and R_C are the mass transfer source terms related to the growth and collapse of the cavitation bubbles, respectively.

In Eq. (5) above, the interphase mass transfer rates per unit volume (R_G and R_C) account for the liquid and bubble phases in cavitation. They are calculated using the growth of a single bubble based on the Rayleigh-Pleasset model [65]. The model assumes no barrier for nucleation; thus, the bubble dynamics can be obtained from the general Rayleigh-Plesset equation as follows [65]:

$$R_b \frac{d^2 R_b}{dt^2} + \frac{3}{2}\left(\frac{dR_b}{dt}\right)^2 = \frac{p_b - p}{\rho_L} - \frac{2\sigma_L}{\rho_L R_b} - \frac{4\nu_L}{R_b}\frac{dR_b}{dt} \quad (6)$$

Where R_b is the bubble radius, ρ_L is the surface tension coefficient of the liquid phase, ρ_L is the liquid density, υ_L is the kinematic viscosity of the liquid phase, p_b is the bubble surface pressure, and p is the local far-field pressure.

Figure 8 shows the geometry of the liquid pool used in the ultrasonic analysis. In Figure 8, the ultrasonic probe has a diameter of 20 mm, an amplitude, A = 10 microns, and a resonant frequency, f = 17.5 kHz. The flow field and cavitation region profiles are shown for two different times in Figures 9 and 10, respectively. It can be seen from Figure 10 that though the predicted ultrasonic cavitation region is relatively small, the acoustic streaming is strong (see Figure 9) and thus the created/survived bubbles/nuclei are transported into the bulk liquid quickly.

Figure 8: A356 liquid pool (the ultrasound probe is shown in the middle of the pool) [58, 61-62].

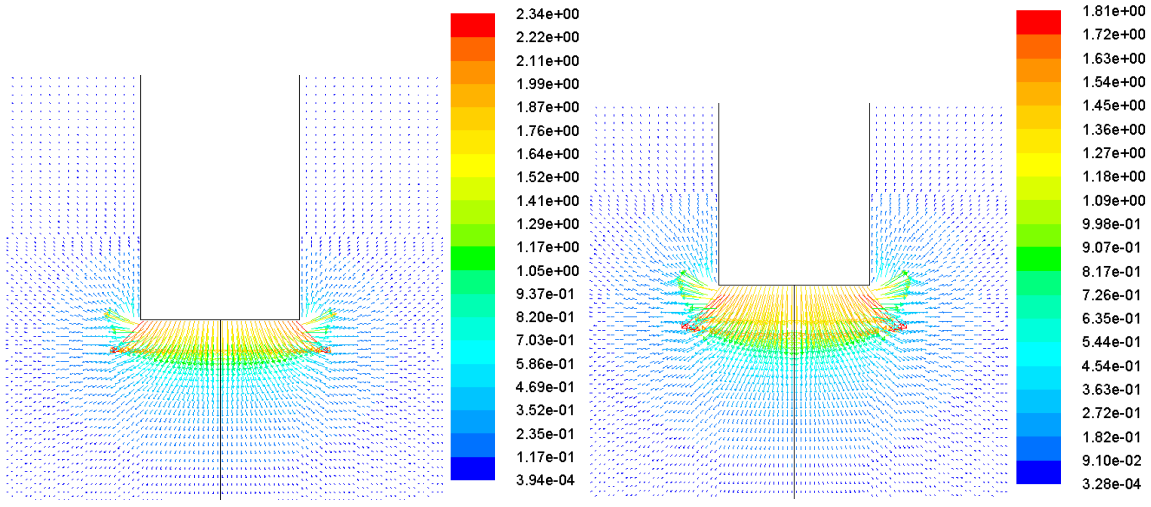

t = 8.8e-06 s **V, m/s** t = 2.0e-05 s **V, m/s**

Figure 9: Flow induced by ultrasound: Flow field (velocity vector) [58, 62-63].

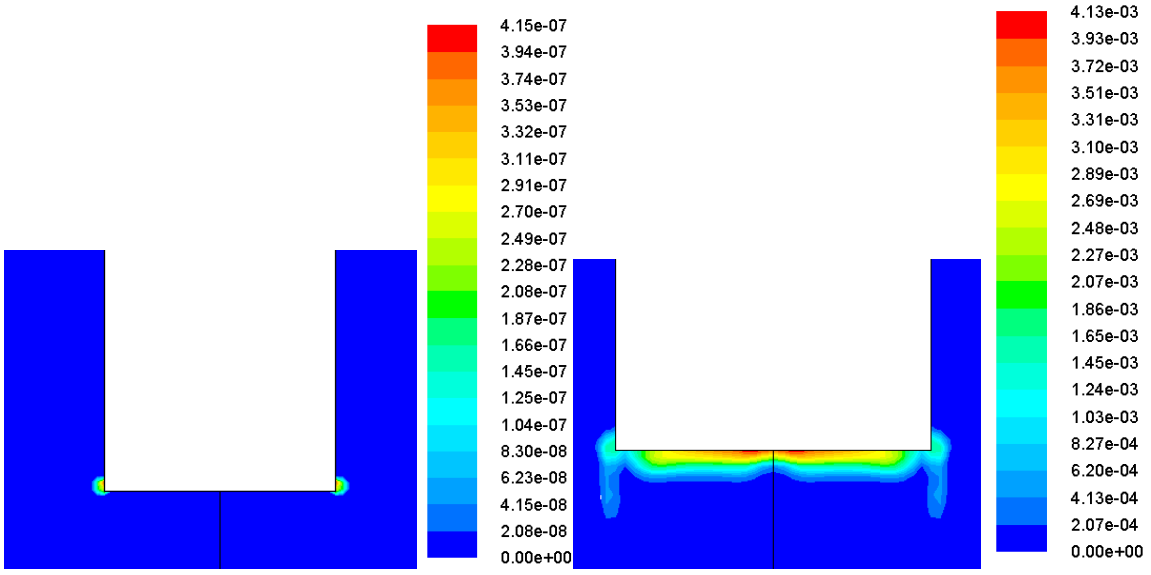

(a) t = 8.8e-06 s (b) t = 2.0e-05 s

Figure 10: Cavitation induced by ultrasound. Legends show the volume fraction of cavities/bubbles/potential nuclei (cavitation region) [58, 62-63].

Figure 11 show the predicted microstructure in the presence of UST. The mesoscopic model developed by Nastac [64, 66] was applied to include the effect of UST on solidification structure evolution and therefore on grain refinement of alloys. The mesoscopic model includes computations of the grain size and columnar-to-equiaxed transition (CET), as well as of segregation. As it can be seen from Figure 11, the predicted grain size under UST processing is approximately one order of magnitude lower than that without UST. Accordingly, the use of UST will be very beneficial to be used as a physical grain refinement technique, especially in the aerospace industry, where chemical grain refinement is not allowed.

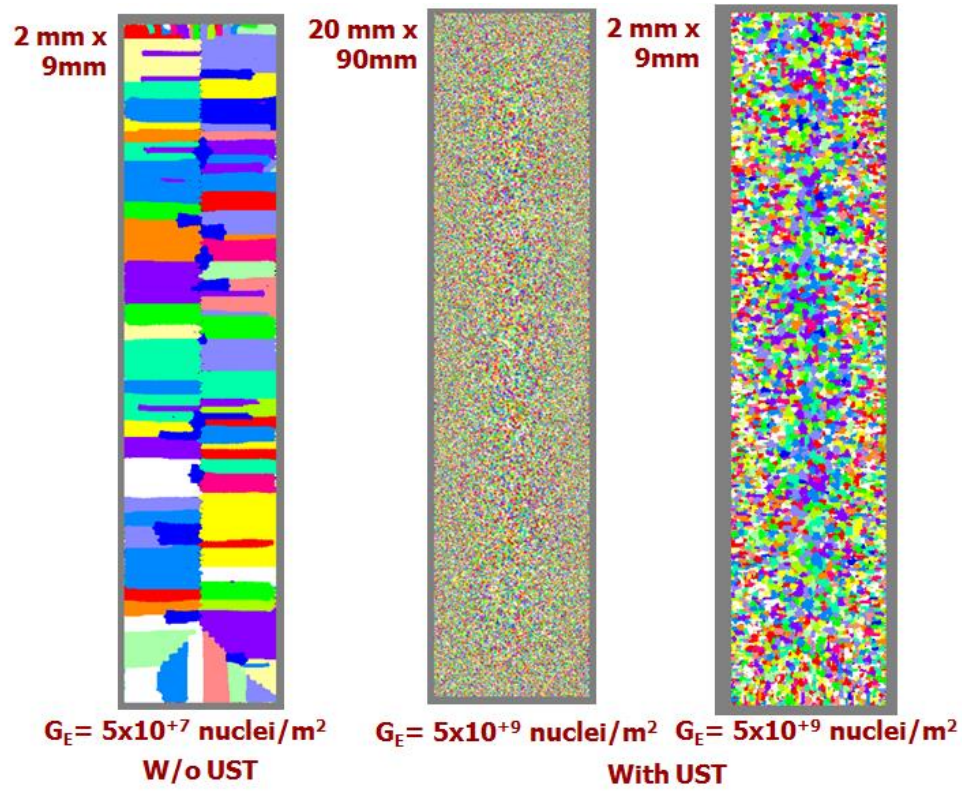

Figure 11: Ultrasonic Treatment: Prediction of Microstructure [59, 64, 66].

2.7 SOLIDIFICATION PROCESSING

The simplicity, economy and flexibility of solidification processes make them attractive methods for the production of particle-reinforced metal-matrix composites. At present, however, there is limited understanding of the phenomena occurring during solidification of these advanced materials. Nucleation and refinement of crystalline phases, physical and chemical interactions between dispersed particles and solidifying interfaces, and buoyancy-driven movement of the particles are areas where a knowledge base is beginning to be formed. Ultimately, the understanding of solidification processes in metal-matrix composites must become complete enough that microstructures can be tailored for specific applications.

In the area of solidification processing, there is a strong desire for a cost-effective and reliable process that enables efficient dispersion of NPs in metal melts for the production of high-performance bulk Mg MMNCs [60].

A judicious selection of solidification process, matrix composition and dispersion method can produce new matrix structures and impart to the composite a unique set of useful engineering properties that are difficult to obtain in conventional monolithic materials. Specifically, the combination of conventional casting processes and the use of inexpensive particles as reinforcements have led to a significant decrease in cost and to the large-scale production of cast metal-matrix particle composites. The formation of solidification microstructures in cast particulate composites is mainly influenced by four phenomena: nucleation (or its absence) on particles; particle pushing by the solidification front; particle settling in the melt; and chemical reactions between particles and the matrix [61].

The difficulty in understanding structure formation in composites is largely due to the unrestricted mobility of the particles in a solidifying melt and the associated disturbances in the distribution of particles. These unsteady-state phenomena render quantification of structure formation inherently more complex in particulate composites than in fiber-reinforced composites, where the analysis is facilitated by a regular stacking of fibers fixed in space.

A consistently observed feature of all solidification microstructures of metal-ceramic particles composites is that certain primary phases, such as the α-phase in aluminum alloys, tend to push the dispersed particles into the residual melt during solidification.

2.8 SUMMARY

Metal matrix composites reinforced with ceramic nanoparticles, termed metal matrix nanocomposites (MMNCs), can overcome the disadvantages of conventional metal matrix composites, such as poor ductility and low fracture toughness. The properties of MMNCs could be significantly improved with a small amount of nanoparticles. There are numerous possible applications of these materials, market fields ranging from aerospace engineering to military industries.

The processing routes for MMNCs could be divided into ex-situ methods and in-situ methods. Ex-situ methods are usually economically efficient but the particles tend to agglomerate due to the poor wettability between the matrix and reinforcement. The reinforcements generated in-situ are usually fine and uniformly distributed, however, they are not cost-effective and have less opportunities than ex-situ reinforcements for complex reactions involved.

At present, ultrasonic cavitation assisted processing appeared to be an effective way among all the fabrication routes. Besides the need for a cost-effective and energy-efficient route for fabrication MMNCs, other issues, such as understanding of the strengthening mechanism and bonding interface reaction, also require to be solved.

3.0 EXPERIMENTAL APPROACH

3.1 MATERIAL APPLIED IN THE EXPERIMENTS

3.1.1 MATRIX: ALUMINUM ALLOY

Aluminum alloy A356 was selected as the metallic matrix because it is readily castable and widely used. It has very good mechanical strength, ductility, hardness, fatigue strength, pressure tightness, fluidity, and machinability. This alloy is used in many industrial applications such as airframe castings, machine parts, truck chassis parts, aircraft and missile components, and structural parts requiring high strength.

The typical chemical composition of an A356 alloy is shown in Table II.

Table II: Nominal chemical composition of matrix alloy A356

Element	Si	Fe	Cu	Mn	Mg	Zn	Ti	Al
wt. %	6.5-7.5	0.20	0.20	0.10	0.25-0.45	0.10	0.20	balance

3.1.2 REINFORCEMENT MATERIALS

The ceramic nanoparticles used in this study were β-SiC and Al_2O_3. The properties are shown in Tables III and IV, separately. Among various types of ceramic particles such as oxides, nitrides, or carbides, Al_2O_3 and SiC are widely used as reinforcement particles due to their relatively good thermal and chemical stability as compared to other types of reinforcements [9, 10].

Table III: SiC nanoparticle parameters

Commercial Name	Silicon Carbide (Beta)
Purity	97.5%
Average Particle Size	45-55 nm
Color	Grayish White
Density	3.22 g/cm^3
Morphology	Spherical

Table IV: Al_2O_3 nanoparticle parameters

Commercial Name	Al_2O_3, Gamma
Purity	>99%
Average Particle Size	20 nm
Color	White
Density	3.890 g/cm^3
Morphology	Spherical

3.2 EXPERIMENT SETUP

Figure 12 shows the ultrasonic processing system available at the Solidification Laboratory, the University of Alabama at Tuscaloosa. The main parameters of the ultrasonic equipment are: maximum power, P=2.4 kW and resonant frequency, f =18 kHz. An induction furnace with a capacity of 6 lbs was used to melt the A356 alloy. A quartz tube with an adjustable switch was used to inject the ceramic nanoparticles just beneath the ultrasonic probe, and the nanoparticles were blown into the melt by Ar gas in a 5 min time-frame, in this way, nanoparticles can be injected into the melt slowly under control and no air contamination was guaranteed. The A356 molten pool was protected by Argon gas atmosphere at the same time. A temperature probe was used to monitor the melt temperature to control the superheat. To cast high quality tensile specimen, steel mold was selected because it can offer good complexity, high cooling rate, and smooth casting surface. The permanent metal mold can be preset to a well-controlled temperature in order to study the effects of different mold temperature and cooling rates. The specimen extracted from the metal mold (as shown in Figure 12) is tested on the tensile test machine. The dimensions of the specimen are 2 inches length and 0.5 inch diameter. The parameters of the ultrasonic stirring technology were determined using a UST software tool previously developed and validated [63]. The UST analysis tool is capable to model acoustic streaming and cavitation.

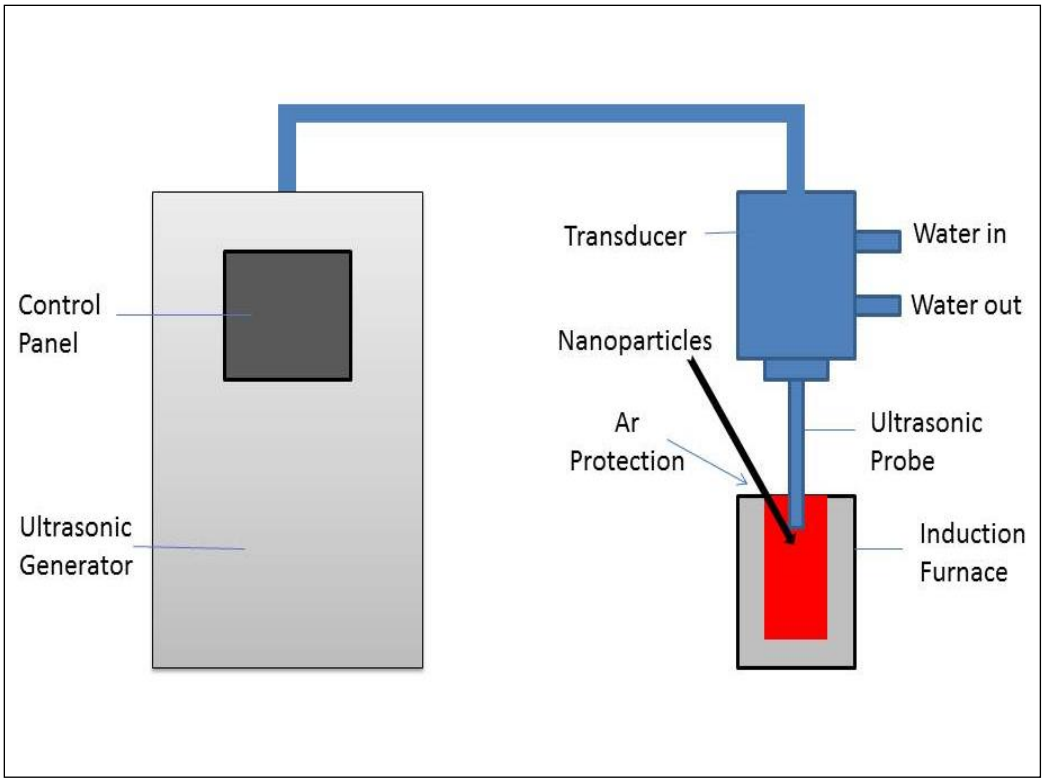

Ultrasonic Processing System

4 kW Ultrasonic Generator

Metal Mold (with generator)

Metal Mold Test Specimen

Figure 12: UST-induction furnace equipment and metal mold available at the Solidification Laboratory, UA.

3.2.1 SCANNING ELECTRON MICROSCOPY ANALYSIS

Microstructure examinations were carried out using scanning electron microscopy (SEM). Specifically, Field Emission Scanning Electron Microscope JEOL JSM-7000F, which can provide high-resolution performance were used to detect the presence of nanoparticles in the bulk A356 nanocomposites sample. Kevex energy dispersive x-ray spectroscopy (EDS) system and X-ray mapping were also utilized to characterize chemical elements and their distribution.

3.3 EXPERIMENT PROCEDURE

A brief description on the experimental procedure is presented below:

1. Weigh the materials we need. Usually 5 lbs A356 alloy will be cut and weighed, 1 wt% nanoparticles will be weighed accordingly.
2. Preheat the permanent metal mold to the desired temperature. (350 ℃)
3. Preheat the A356 ingots (5 lbs) to eliminate any moisture and other contaminants, and then add them in the furnace for melting.
4. After the alloy is melted, insert the Nb (Niobium) ultrasonic probe about 2 inches beneath the melt surface, perform ultrasonic stirring at 1.75 kW (about 70% of the maximum power-2.4kW) and 18 kHz resonant frequency, as shown in Figure 13. The utilized power is sufficient to create cavitation into the melt.
5. The 1 wt% nanoparticles were weighed and then added into a quartz tube before the experiments. When the A356 melt completely, the quartz tube was inserted into the cavitation area of the melt, which is just beneath the ultrasonic probe; meanwhile, the ultrasonic probe was applied to the melt and the power was turned on. At one end of the tube, Argon was applied to inject Al_2O_3 or SiC nanoparticles into the melt. 1 wt. % nanoparticles were injected into the melt during a 5 min time-frame.
6. A higher pouring temperature of 750℃ was used to minimize the formation of metal-mold filling defects including cold-shuts and decrease the viscosity of the melt.
7. The casting was extracted from the metal-mold after cooling in the mold for at least 30 min. After it completed cooled down, mark it with proper description.

Figure 13: Ultrasonic Processing System.

8. For microstructural study, samples of as-cast bulk MMNCs were mounted, mechanically polished down to 1 μm, and etched by Keller's reagent (2 ml HF (48%), 3ml HCl (conc.), 5ml HNO3 (conc.) and 190 ml water).

During the whole process, the temperature of the molten A356 alloy was monitored by a thermocouple, the pouring temperature and processing temperature were ensured to be in the range of our processing parameters. If the temperature is much higher than 750℃, the structure of the molten A356 will be changed, which is harmful to the experimental results. At the same

time, the molten metal was protected from air contamination by Argon gas continuously. We started the Argon gas as soon as the A356 started to melt, and stopped just before pouring, in this way, minimum air contamination could be guaranteed so that porosity brought by air should be controlled at the lowest level.

4.0 RESULTS AND DISCUSION

4.1 OPTICAL MICROSTRUCTURE ANALYSIS

Figures 14-16 show the microstructure of the as-cast A356 alloy and UST treated Al_2O_3/SiC reinforced A356 nanocomposites cast in the metal molds at magnifications of 50x, 200x and 1000x, respectively. From these pictures, it is clear that the grains were refined after the ultrasonic treatment compared to the sample without any treatment. Also, the grain size of the samples with nanoparticles are smaller than the samples without them. In addtion, a comparision between Figure 14(c) and 14(d) showed that with the increase of the weight percent of the SiC nanoparticles, the grain sizes become even smaller. The reason of this increase migth be because the nanoparticles will block the grains from growing bigger as they already dispersed on the area, the grain cannot bypass the particles to further grow. In addition, the more nanoparticles in the melt, the higher nucleation potential of the melt. According to Table V, the SDAS decreased by 11.3% after ultrasonic treatment, and with the addition of nanoparticles, SDAS even decreased by more than 36.2% than in the standard A356 alloy. Also, the eutectic structures are more refined after UST processing (see Figure 15). In addition, the amount of porosities after ultrasonic treatment has been reduced significantly. The degassing effect of the ultrasonic treatment is clearly shown in Figures 14-16.

According to Hall-Petch strengthening equation:.

$$\sigma_y = \sigma_0 + \frac{k_y}{\sqrt{d}} \tag{7}$$

Where σ_y is the yield stress, σ_o is a materials constant for the starting stress for dislocation movement (or the resistance of the lattice to dislocation motion), k_y is the strengthening coefficient (a constant unique to each material), and d is the average grain diameter or average arm spacing of the microstructure under consideration.

A more detailed equation with the addition of eutectic phase fraction, f_E, can be written as following:

$$\sigma = f_p\ \sigma_p + f_E\ \sigma_E \qquad (8)$$

Where σ is the overall mechanical yield strength, f_p is the fraction of primary dendritic phase, f_E is the fraction of eutectic phase , σ_p is the yield stress of primary dendritic phase, σ_E is the yield stress of eutectic phase. Both σ_p and σ_E are inversely proportional to the size of microstructure as shown by Eq. (7).

As shown by Eqs. (7) and (8), the smaller the sizes of the primary and euctectic morphologies, the bigger the mechanical strength. This is verified by the experimental measurements (see the microstructures and mechanical properties in Table V and VII).

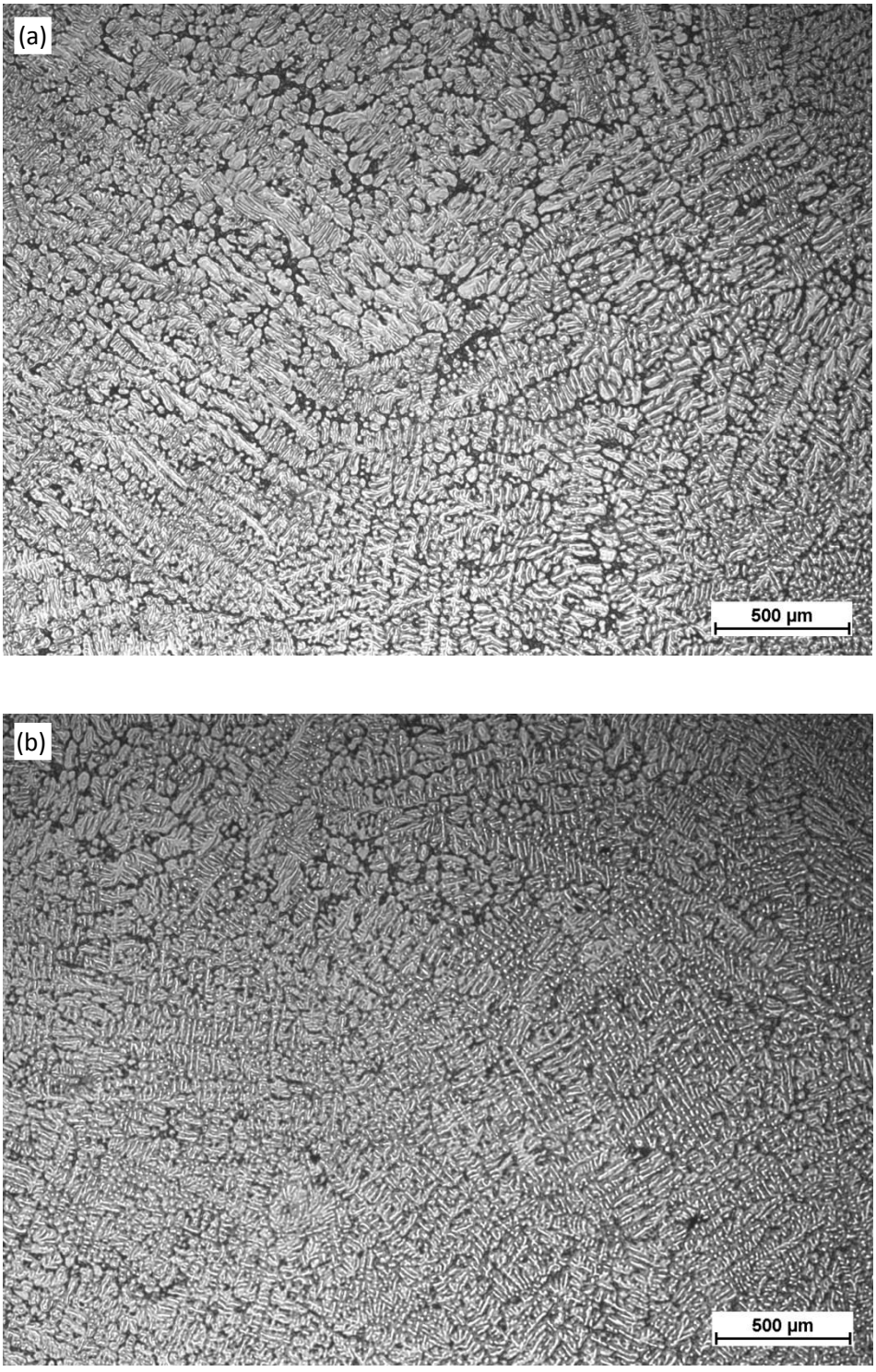

Figure 14: Microstructures of A356 alloy under magnification of 50X (metal-mold samples): (a) Standard (b) UST+1%Al_2O_3 (c) UST+0.7%SiC (d) UST+1%SiC

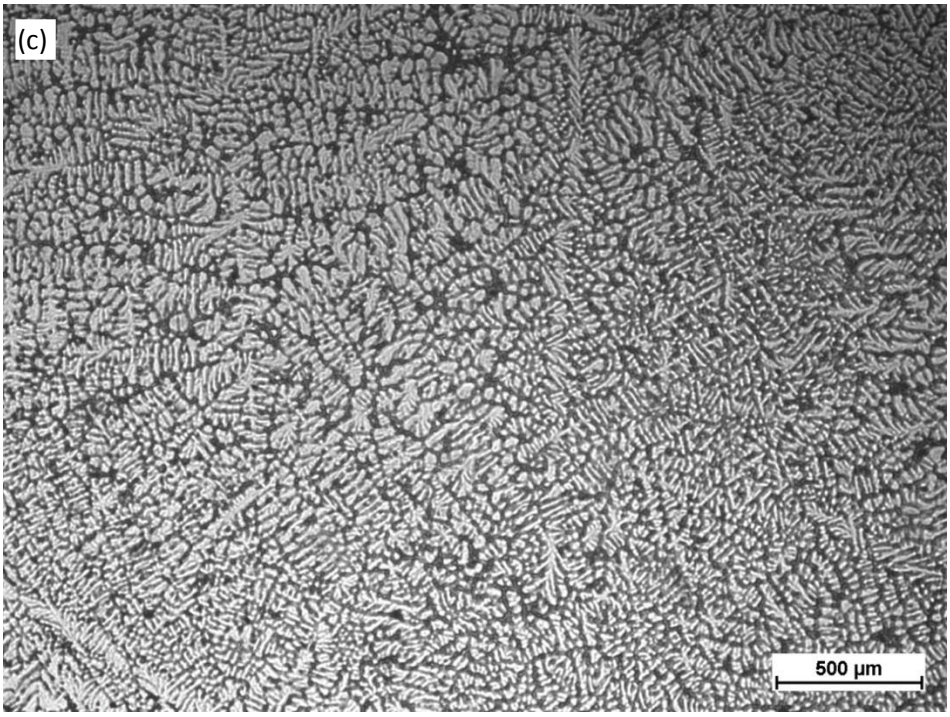

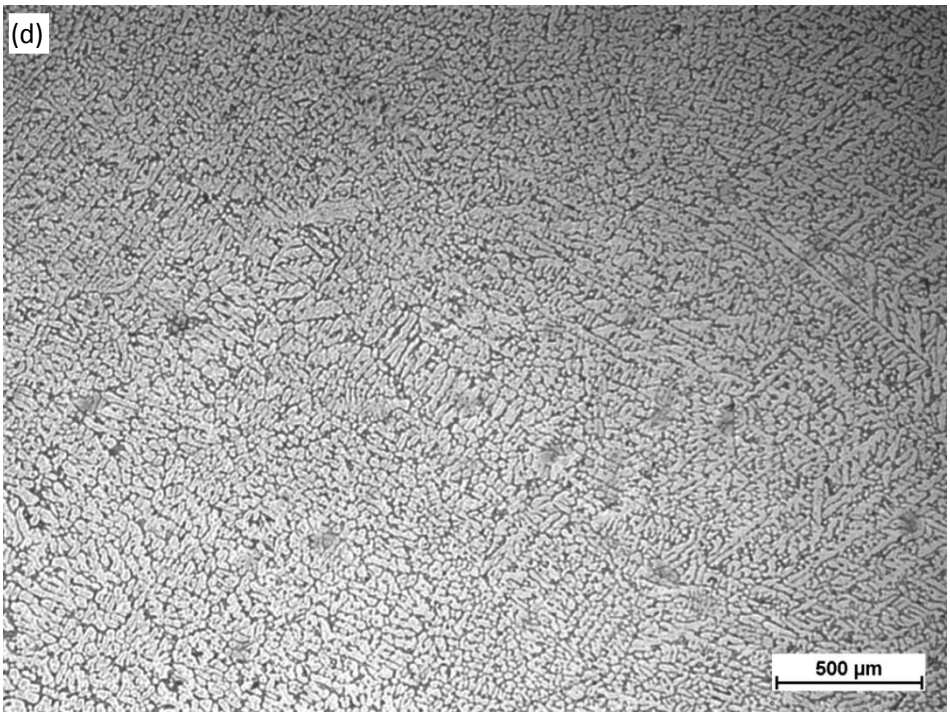

Figure 14 (continued): Microstructures of A356 alloy under magnification of 50X (metal-mold samples): (a) Standard (b) UST+1%Al_2O_3 (c) UST+0.7%SiC (d) UST+1%SiC

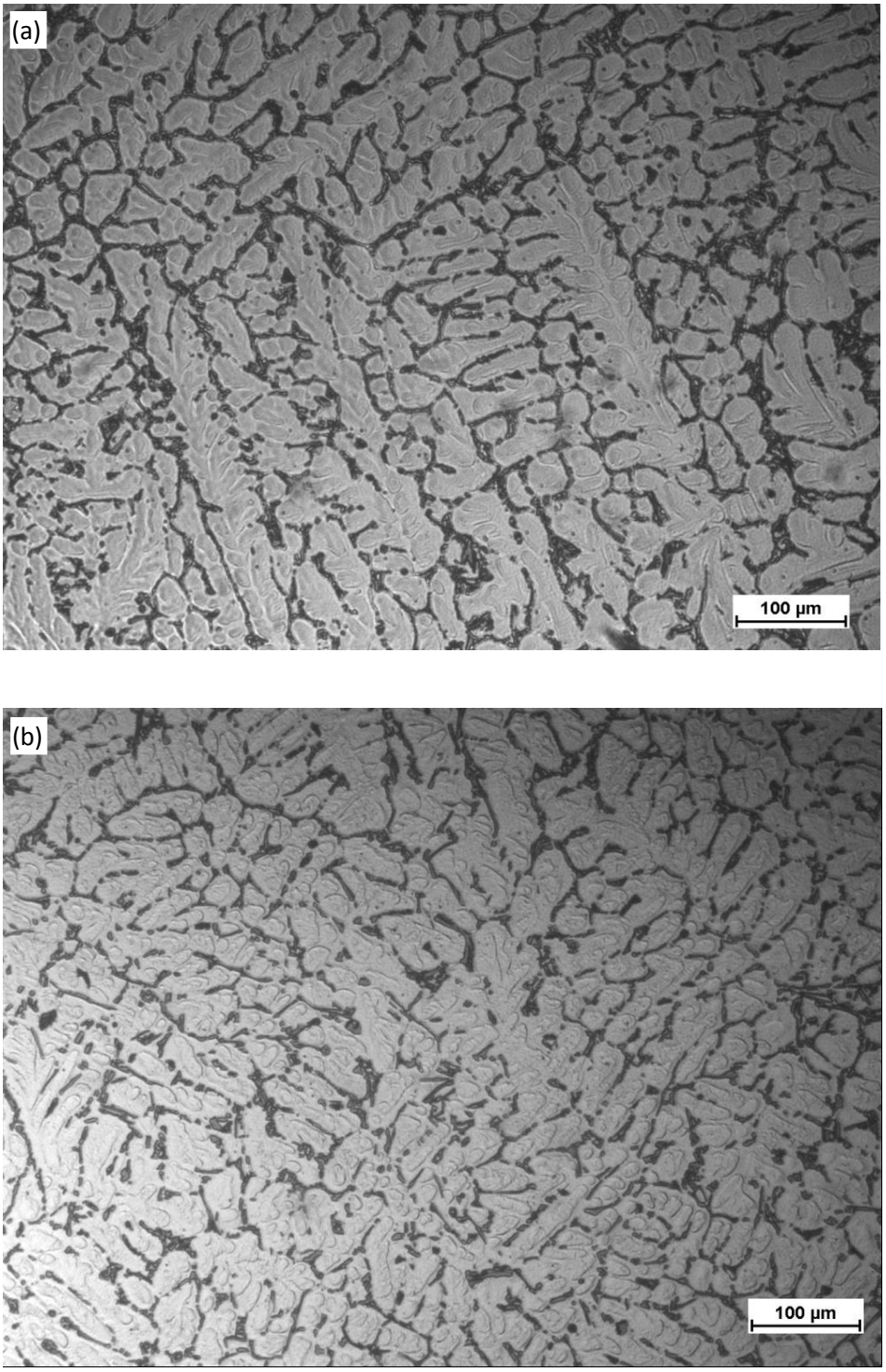

Figure 15: Microstructures of A356 alloy under magnification of 200X (metal-mold samples):

(a) Standard (b) UST+1%Al_2O_3 (c) UST+0.7%SiC (d) UST+1%SiC

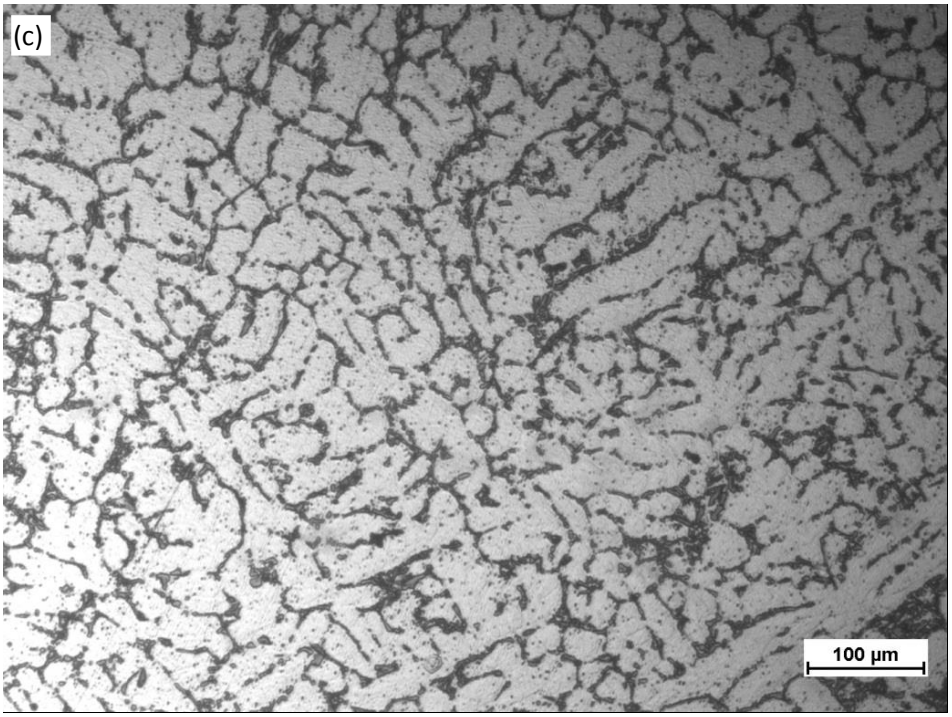

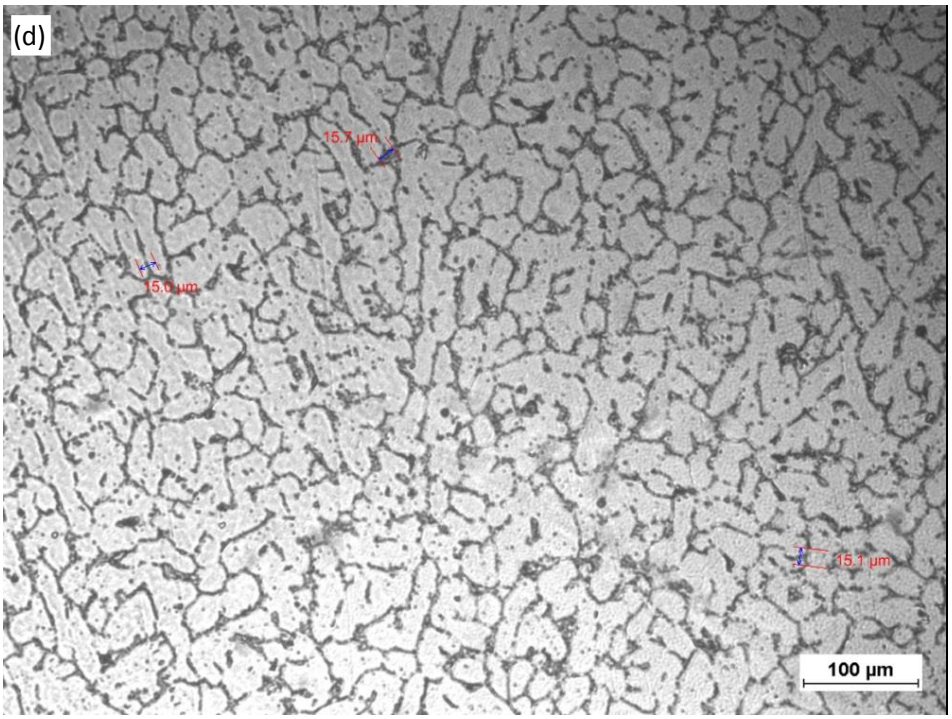

Figure 15 (continued): Microstructures of A356 alloy under magnification of 200X (metal-mold samples): (a) Standard (b) UST+1%Al_2O_3 (c) UST+0.7%SiC (d) UST+1%SiC

Table V: Comparison of SDAS (Secondary Dendrite Arm Spacing) using different processing methods

SDAS (μm)	#1	#2	#3	Average
Standard A356	23.2	28.0	32.1	**27.8**
UST+1%Al_2O_3	20.6	19.1	11.7	**17.1**
UST+0.7%SiC	16.7	24.0	12.8	**17.8**
UST+1%SiC	15.7	15.0	15.1	**15.3**

The eutectic structures are more refined after the UST process, as shown in Figure 16 and Table VI. Table VI shows that with the addition of nanoparticles, the eutectic spacing has increased. In addition, the amount of porosities after ultrasonic treatment has reduced significantly, as shown in Figures 14-16. The degassing effect of ultrasonic can be probably illustrated according to the results.

Figure 17 shows that the microstructures of UST+nanoparticles cast into a pouring cap (silica sand mold) that solidify at relatively low cooling rates when compared with the samples cast into the metal-mold. The microstructures processed under UST and with nanoparticles are more refined when compared with the standard A356 alloy.

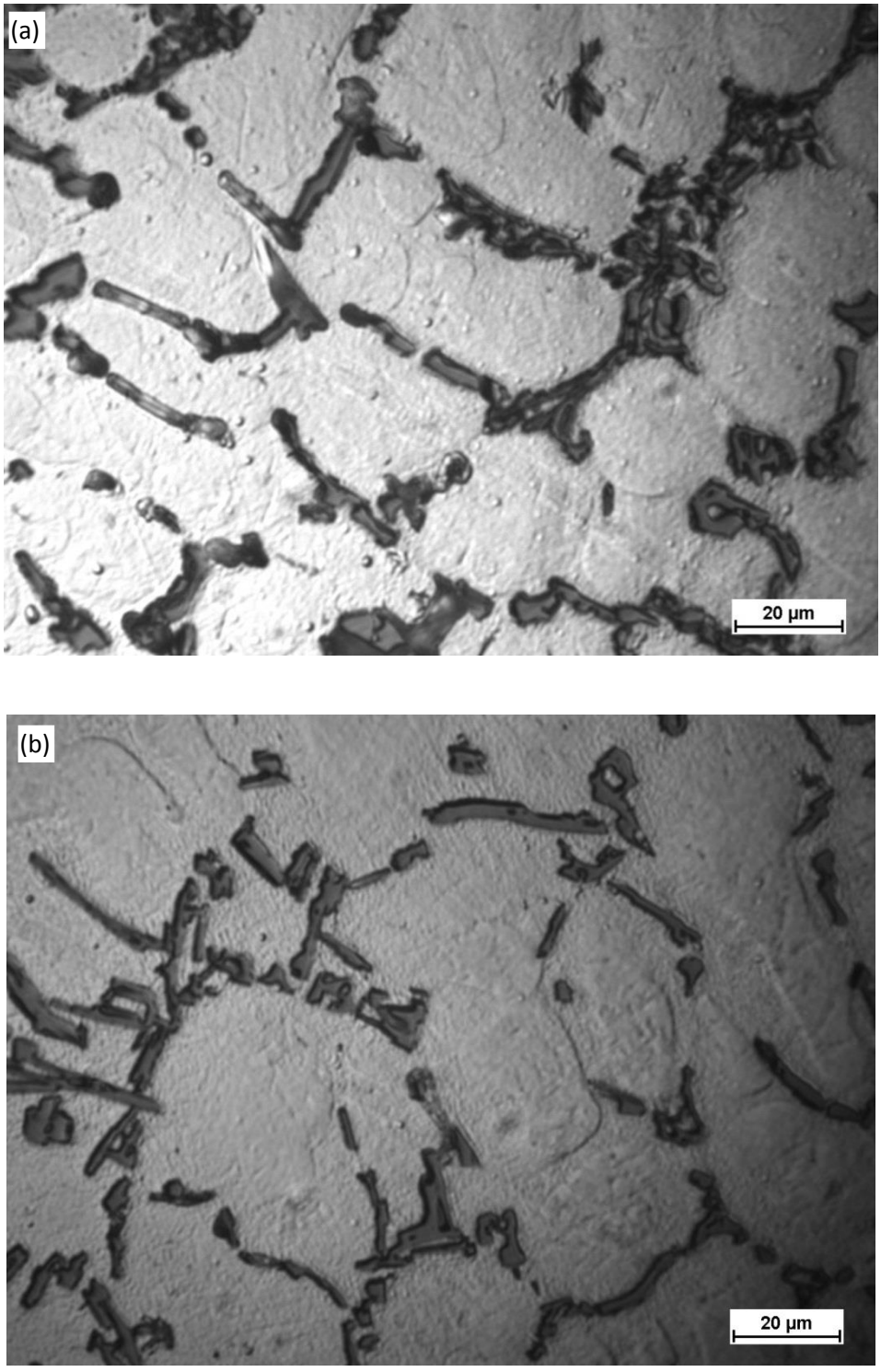

Figure 16: Eutectic microstructures of A356 alloy under magnification of 1000X (metal-mold samples): (a) Standard (b) UST+1%Al_2O_3 (c) UST+0.7%SiC (d) UST+1%SiC

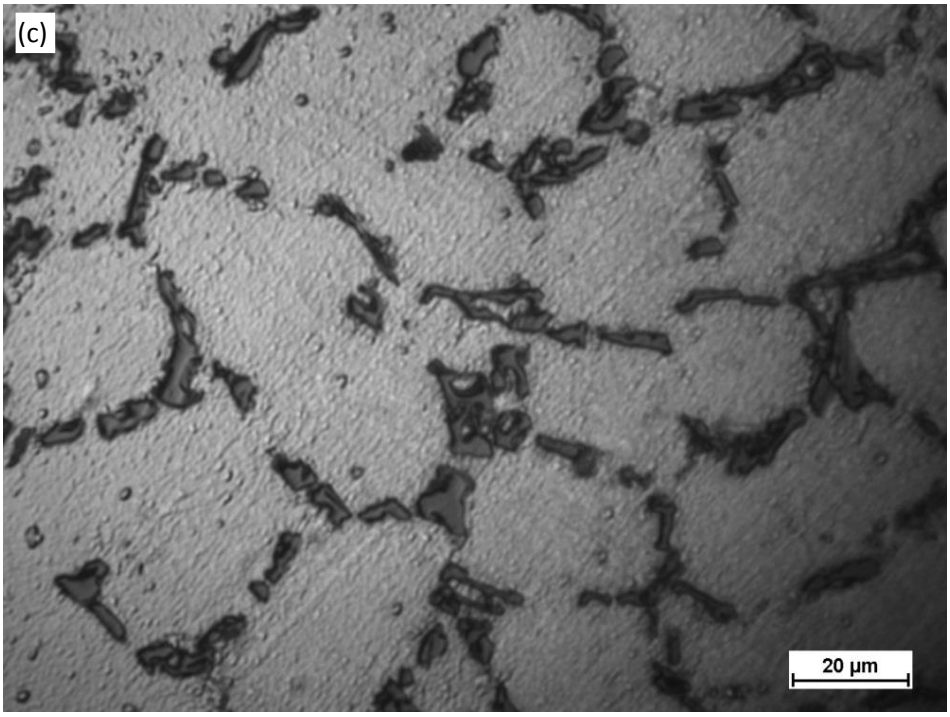

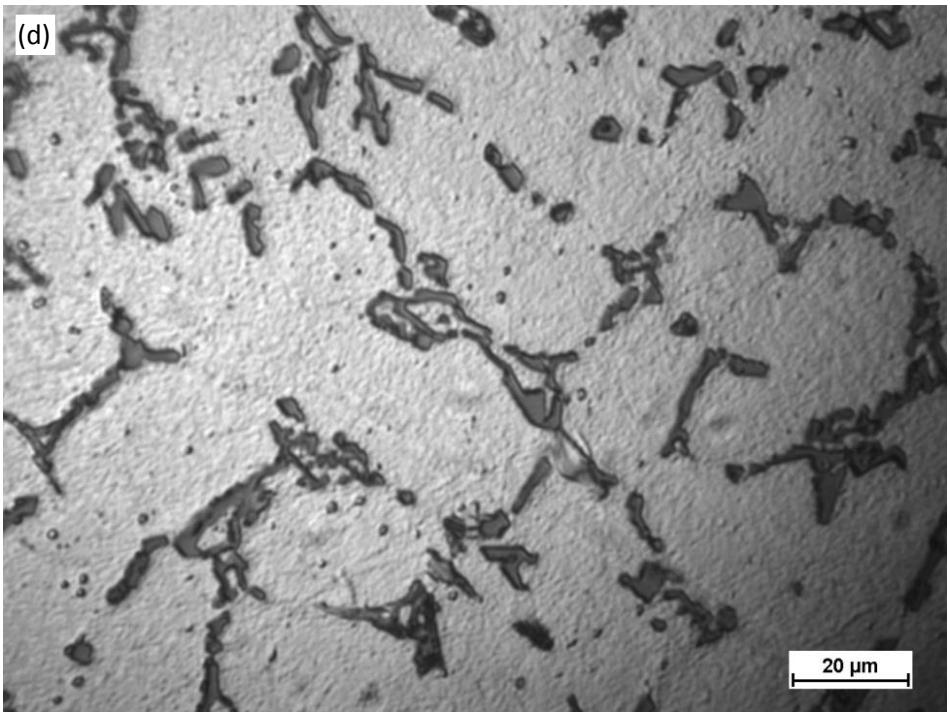

Figure 16 (continued): Eutectic microstructures of A356 alloy under magnification of 1000X (metal-mold samples): (a) Standard (b) UST+1%Al_2O_3 (c) UST+0.7%SiC (d) UST+1%SiC

Table VI: Comparison of eutectic spacing of all processed materials

Eutectic Spacing (µm)	#1	#2	#3	Average
Standard	2.4	2.1	1.8	2.1
UST+1%Al_2O_3	4.6	3.3	2.4	3.4
UST+0.7%SiC	4.1	4.2	3.6	4.0
UST+1%SiC	3.2	4.0	4.4	3.9

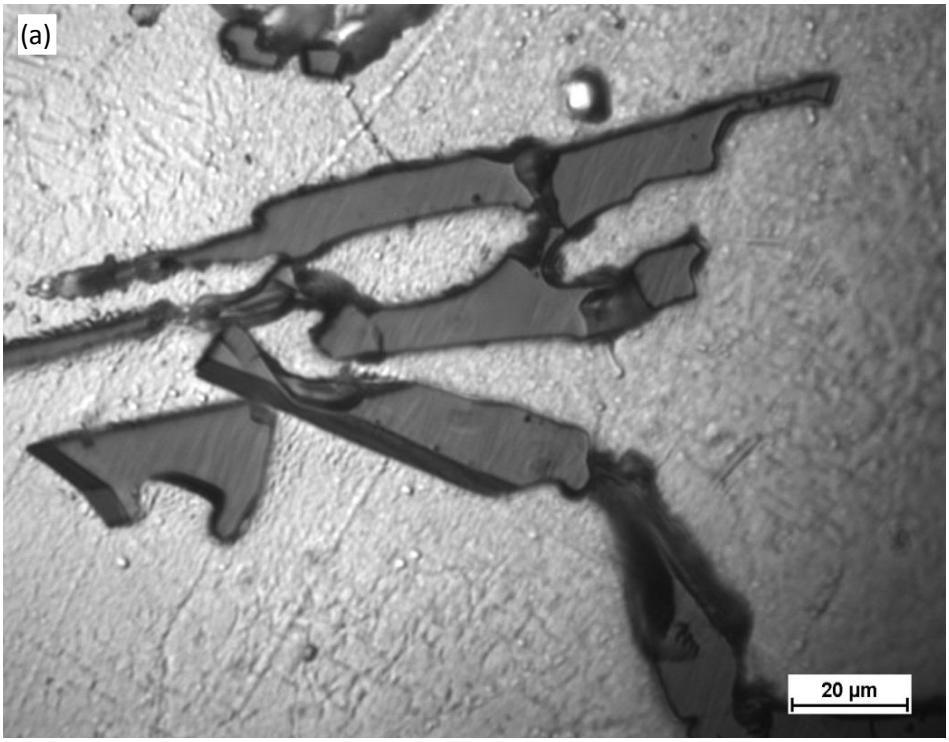

Figure 17: Microstructures of A356 alloy poured in the cooling cup (sillica sand molds): (a) standard A356 (b) UST+1%Al_2O_3 (c) UST+0.7%SiC (d) UST+1%SiC.

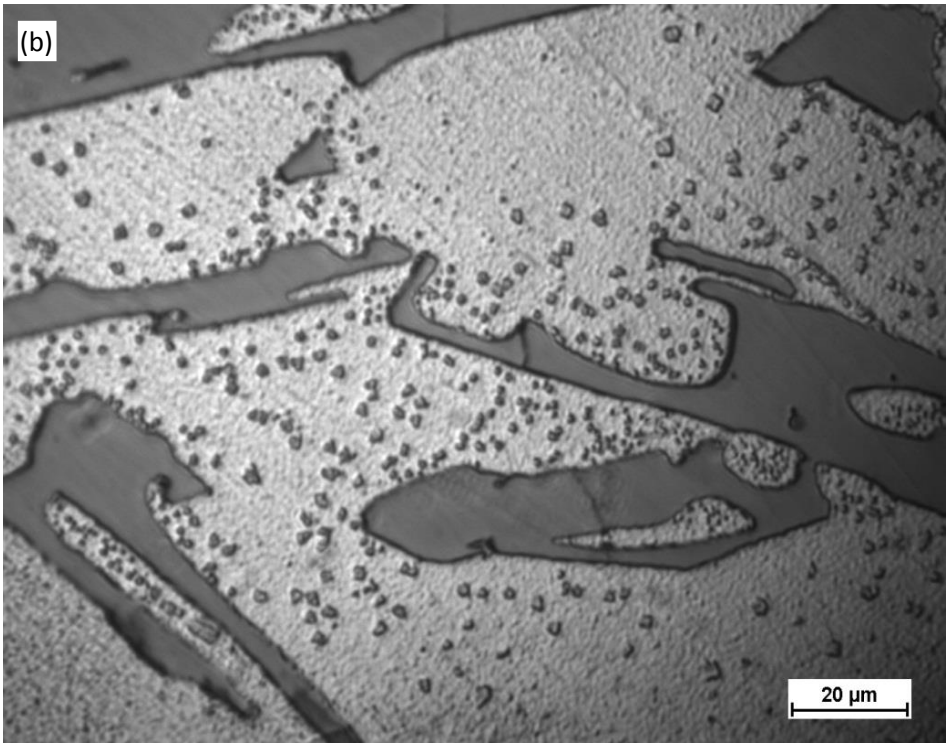

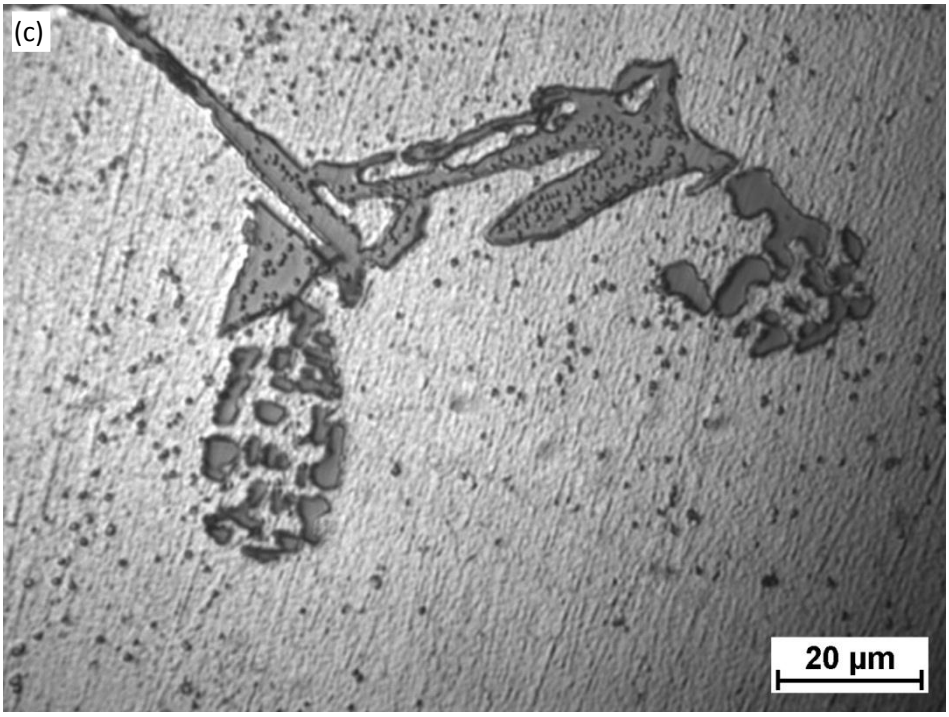

Figure 17 (continued): Microstructures of A356 alloy poured in the cooling cup (sillica sand molds): (a) standard A356 (b) UST+1%Al_2O_3 (c) UST+0.7%SiC (d) UST+1%SiC.

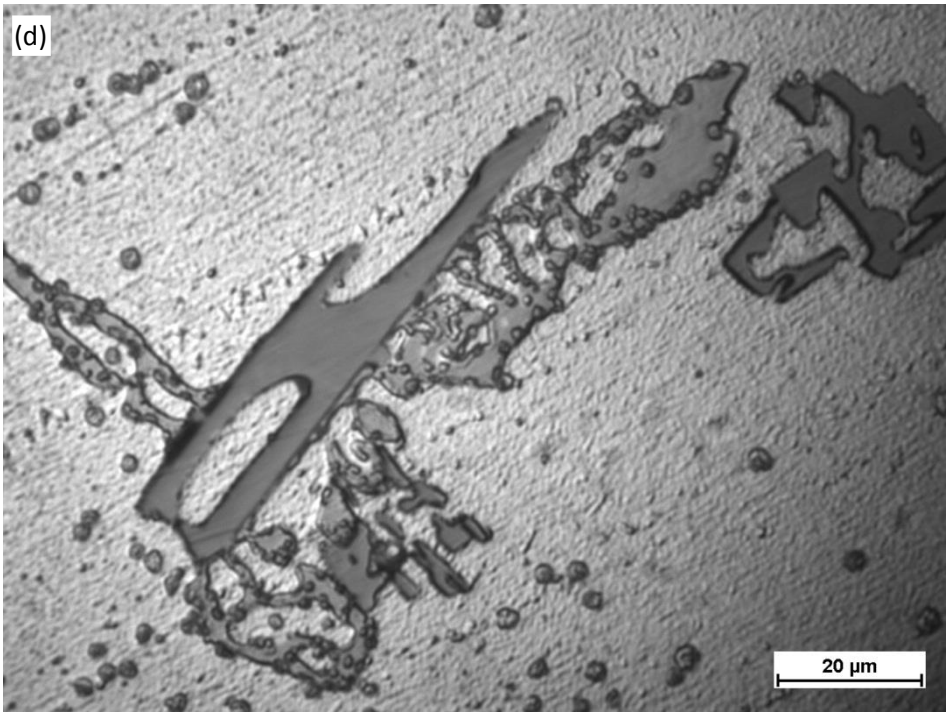

Figure 17 (continued): Microstructures of A356 alloy poured in the cooling cup (sillica sand molds): (a) standard A356 (b) UST+1%Al_2O_3 (c) UST+0.7%SiC (d) UST+1%SiC.

4.2 MECHANICAL PROPERTIES OF NANOCOMPOSITES

After the T6 heat treatment (solution heat treatment for 4h at 932F and aging heat treatment for 4h at 311F), a mechanical testing was done to measure tensile strength, yield strength and elongation, see table VII. Compared to as-cast A356, the tensile strength of 1wt% Al_2O_3, 1wt% SiC, remelt 1wt% SiC nanocomposites increased by 15.3%, 24.1%, 20.7%, respectively.

At the same time, improvement in elongation can be seen as well in all UST+nanoparticles samples. Furthermore, the A356+SiC nanocomposites performed slightly better than the A356+Al_2O_3, perhaps due to the fact that the samples with Al_2O_3 nanoparticles have more gas

pores than the ones with SiC nanoparticles (see Figure 14-15). These phenomena can be explained by the fact that aluminum is easy to oxidize and after oxidation, the wettability between aluminum and Al_2O_3 nanoparticles became worse.

Table VII: Comparison of mechanical properties using different processing methods

Samples	Tensile Strength(MPa)	Yield Strength(MPa)	Elongation (%)
Standard A356(Degas 3min)	228 ±4	180 ±3	4.0 ±0.3
UST 5min +1% Al_2O_3	263 ±8	196 ±5	6.3 ±0.5
UST+1% SiC	283 ±4	196 ±2	11.2 ±0.9
Remelt UST+1% SiC	275 ±7	190 ±6	6.3 ±0.3

4.3 COOLING CURVE ANALYSIS

Figure 18 show the cooling curves obtained by pouring the melta into a sand mold pouring cup. From the cooling curves presented in Figure 18b, it appears that in all the experiments with UST and addition of nanaparticles, the cooling rates and solidification times are similar. This confirm that all the with UST and addition of nanaparticles experiments have been performed under similar solidification/ cooling conditions. Slightly longer solidification time is shown in Figure 18(a) in the case without the UST processing.

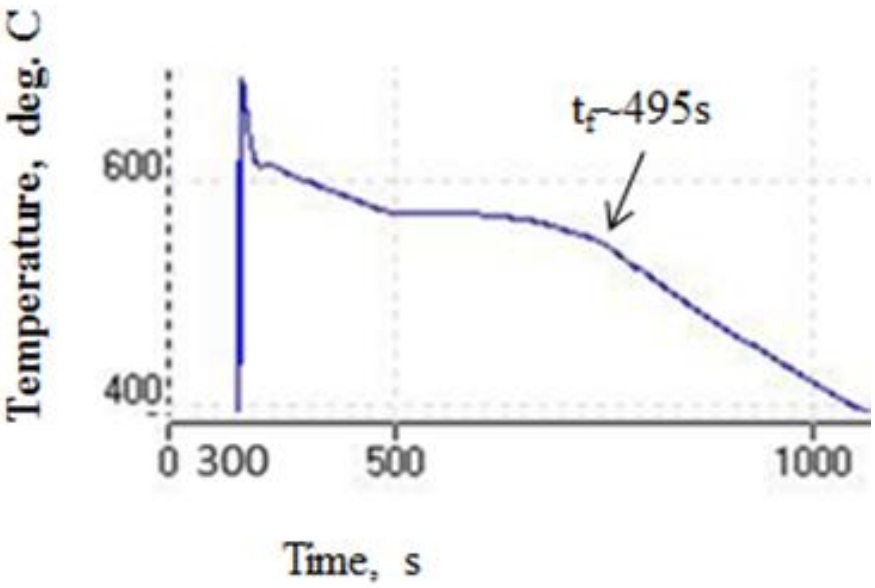

(a)

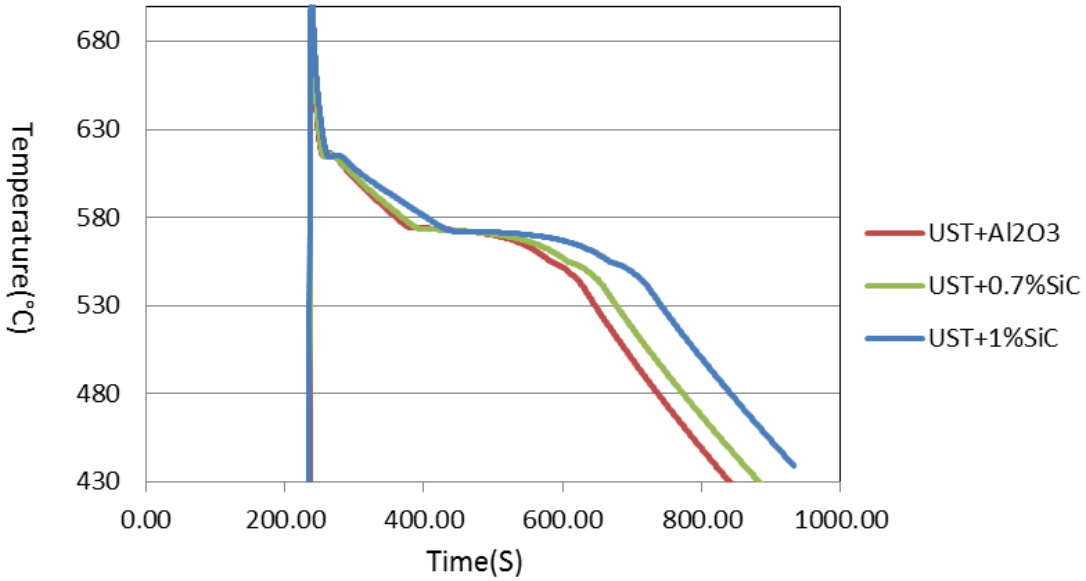

(b)

Figure 18: Cooling curves: (a) w/o UST and (b) UST+1%Al_2O_3, UST+0.7%SiC and UST+1%SiC.

4.4 SEM ANALYSIS OF A356/ 1 WT% SIC SAMPLE

Figure 19 show the distribution of SiC nanoparticles in the A356/ 1 wt% SiC MMNC sample. It can be seen that SiC nanoparticles were well dispersed into the A356 matrix. It also showed that some agglomeration had occurred during the MMNC processing. Further analysis is required to determine the cause of this agglomeration and how to prevent it.

In order to further verify the dispersion of the nanoparticles in the A356 matrix, EDS analysis was also performed. Figure 20 shows the EDS spectrum of the A356 nanocomposites. Aluminum, silicon and carbon were detected in the analysis. It seems that the MMNC process was well protected quite well since no oxygen was detected. Since the average size of the nanoparticles is less than 60 nm, it is very difficult to use EDS-spot analysis on a single particle due to the limitation of the E-beam resolution in this instrument. Therefore, mapping scanning was employed.

Figure 21 shows the distribution of the aluminum (Al), carbon (C), and silicon (Si) elements, respectively. From the elemental distribution of carbon (C) shown in Figure 21, an uniform dispersion of SiC nanoparticles can be observed. Also, the image showing the distribution of Si in Figure 21 clearly demonstrates the presence of the eutectic phase. Further SEM and TEM analyses will be carried out to have a better understanding of the SiC dispersion into the A356 matrix.

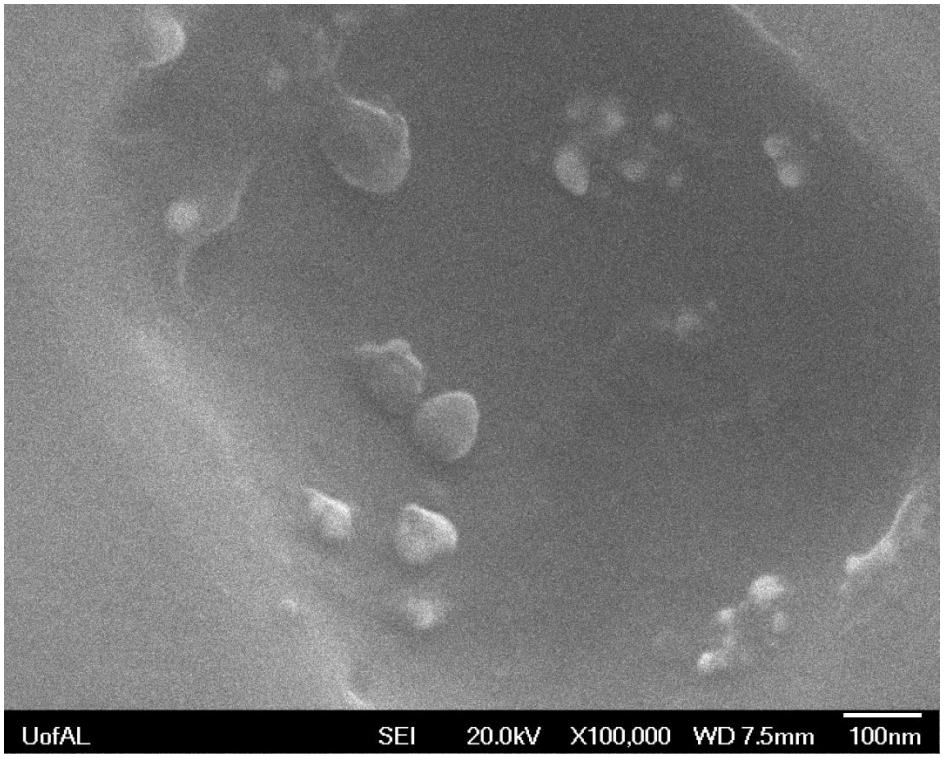

Figure 19: The distribution of SiC nanoparticles in the MMNC sample

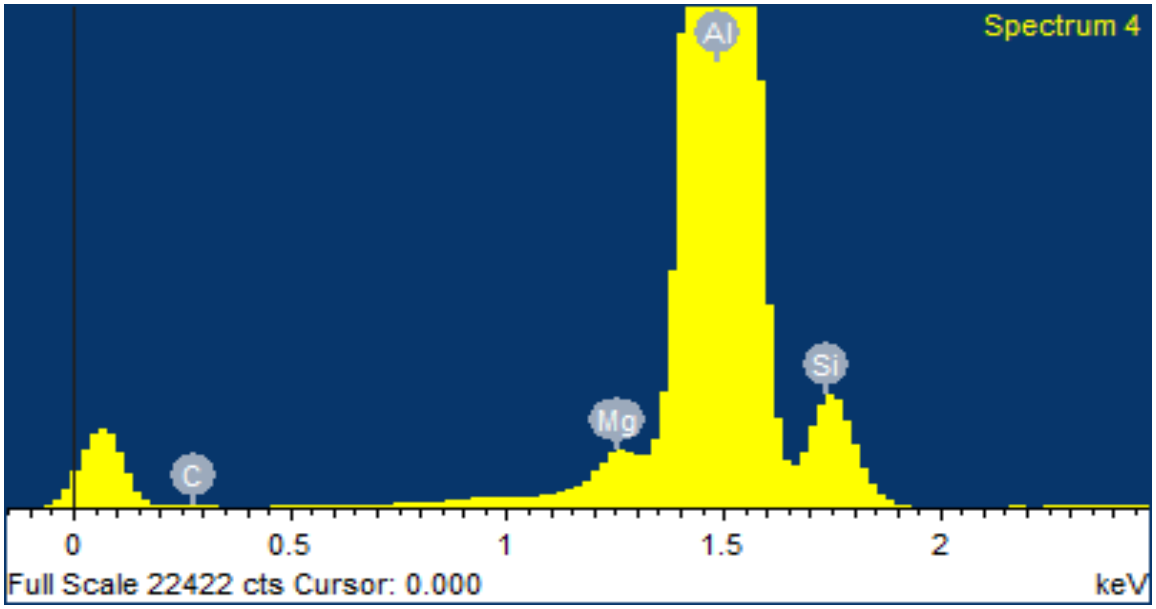

Figure 20: EDS spectrum of A356/1 wt.% SiC nanocomposites

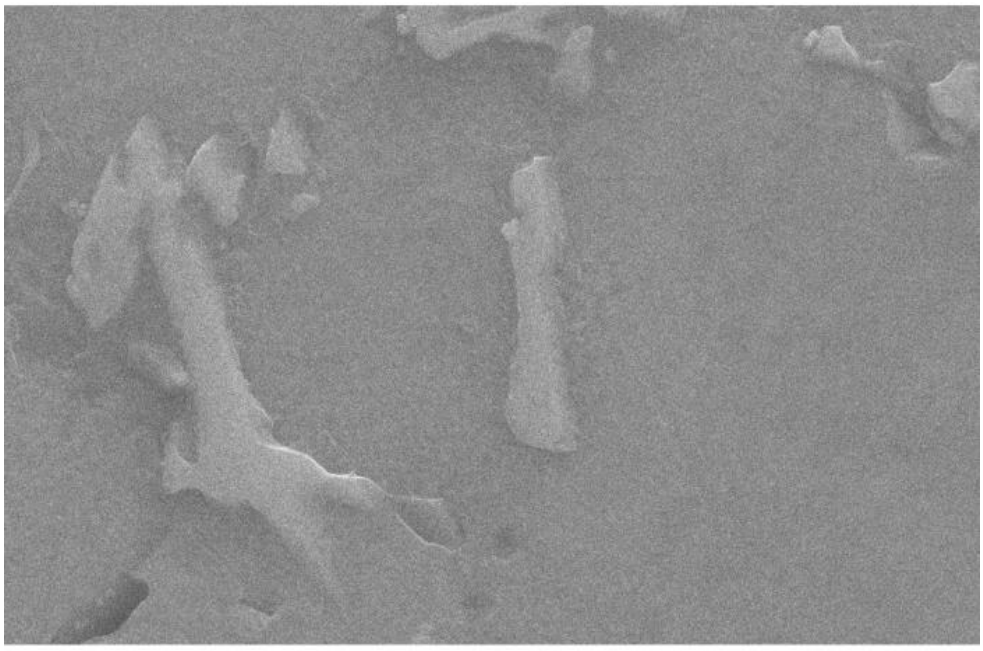

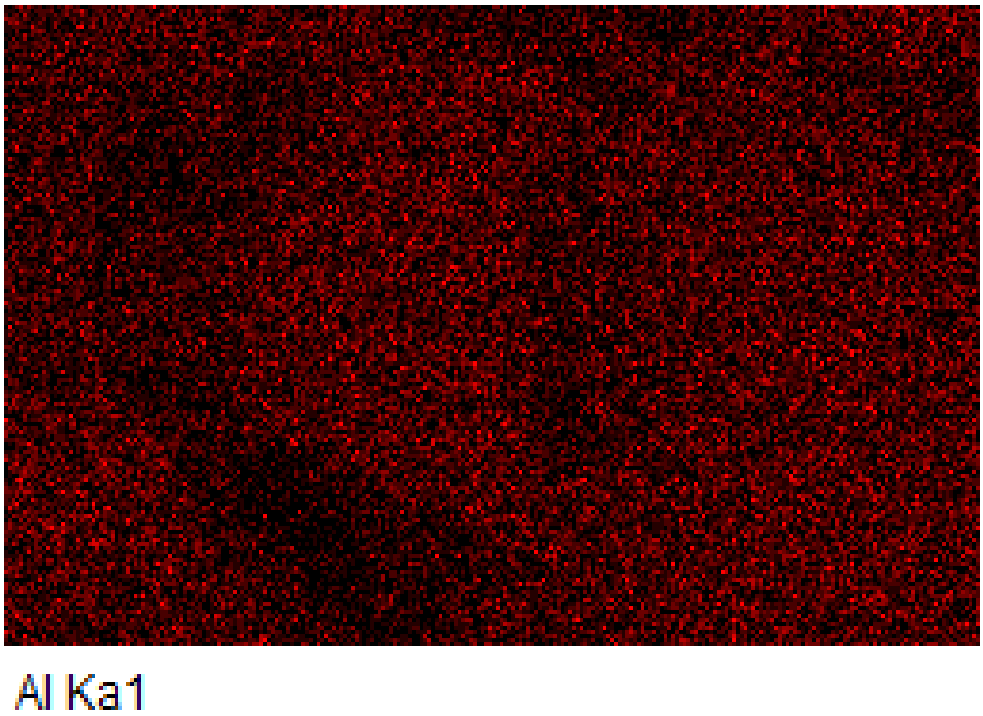

Figure 21: Element distribution of nanocomposites from EDS mapping

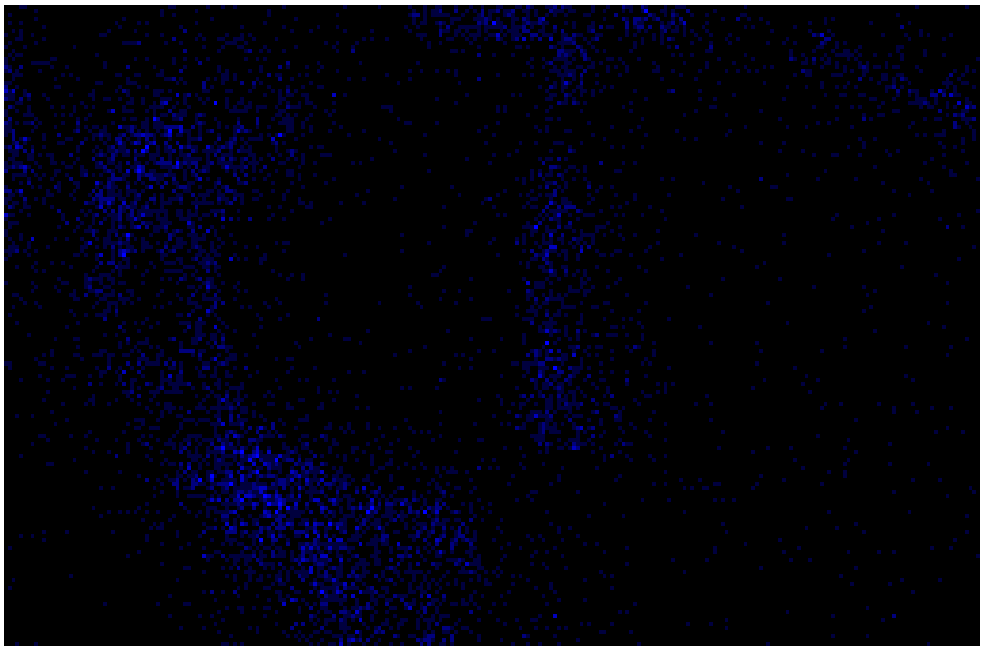

Si Ka1

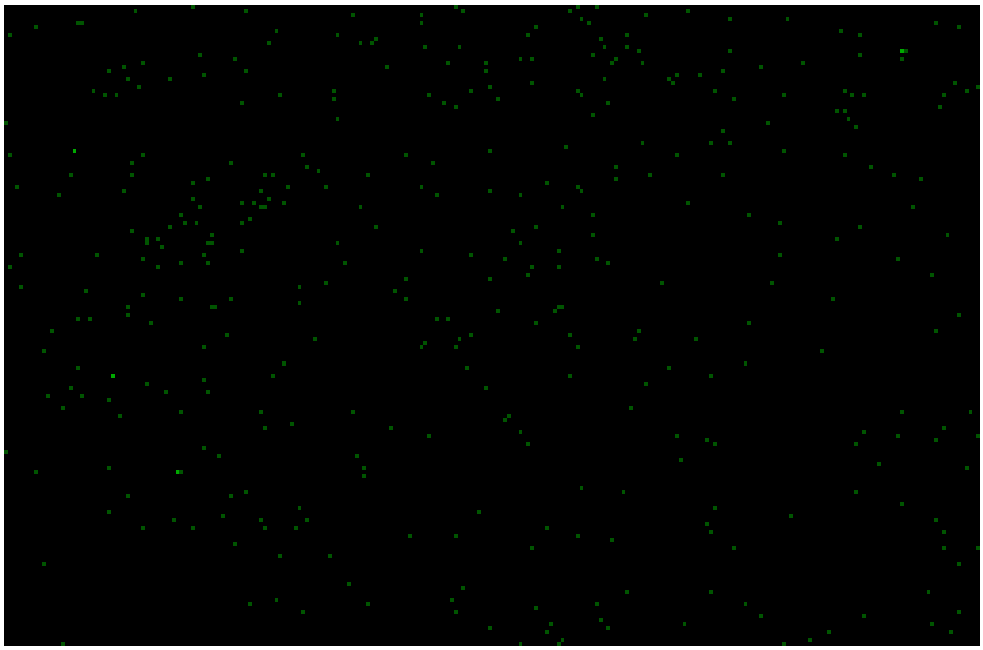

C Ka1_2

Figure 21 (continued): Element distribution of nanocomposites from EDS mapping

5.0 CONCLUDING REMARKS AND FUTURE WORK

5.1 CONCLUSIONS:

The following main effects of ultrasonic treatment on A356 nanocomposites can be seen from the experimental results:

(i) Due to ultrasonic treatment, microstructures were refined by ultrasonic stirring and cavitation; grain size and SDAS decreased, columnar-to-equiaxed-transition (CET) was completely eliminated (as shown in Figures 14-16);

(ii) Ultrasonic degassing of the molten alloy was quite good; this is demonstrated by the observed reduced gas porosity in all samples in Figures 14-16.

(iii) From the cooling curves presented in Figure 18b, it appears that in all the experiments with UST and addition of nanaparticles, the cooling rates and solidification times are similar. This confirm that all the with UST and addition of nanaparticles experiments have been performed under similar solidification/ cooling conditions.

(iv) Nanoparticles can be seen through SEM images, EDS mapping showed three main elements (Al, Si, C) in the nanocomposites; it was shown that agglomeration still exists.

(v) Significanlty improvement in the mechanical properties including tensile strength and yield strength as well as ductility were achieved after adding the ceramic nanoparticles by ultrasonic processing. Hall-Petch strengthening mechanism can be verified by the microstructures and mechanical properties in Table V and VII.

5.2 FUTURE WORK:

Future work will include STEM (Scanning Transmission Electron Microscope) analysis of cast A356 nano-composites to clearly understand the effects of ultrasonic cavitation process on dispersion of nanoparticles and whether the dispersion of nanoparticles is uniform or not after the ultrasonic cavitation and acoustic streaming processing.

i) Optimization of the fabrication process;

ii) Investigation of the influence of different kinds of reinforcement materials on the properties of the nano-composites.

In addition, a CFD (Computational fluid dynamics) model that can simulate the ultrasonic processing of nano-composites, which was recently developed [62-64] will be further refined and validated.

6.0 REFERENCES

[1] L. Hengcheng, S. Yu, and S. Guoxiong, Restraining effect of strontium on the crystallization of Mg_2Si phase during solidification in Al-Si-Mg casting alloys and mechanisms, Mater. Sci. Eng. A 358, (2003), 164-170.

[2] M. A. Gaffar, A. Gaber, M. S. Mostafa, and E. F. Abo Zeid, The effect of Cu addition on the thermoelectric power and electrical resistivity of Al-Mg-Si balanced alloy: A correlation study, Material Science and Engineering A 465, (2007), No 1-2, 274-282.

[3] J.E. Gruzieski and B.M. Closset: The Treatment of Liquid Aluminum-Silicon Alloys, American Society of Foundary, Des Plaines, IL, (1990), 13-15.

[4] G. Ran, J.E. Zhou, and Q.G. Wang, Precipitates and tensile fracture mechanism in a sand cast A356 aluminum alloy, J. Mater. Process. Technol. 207, (2008), 46-52.

[5] E.T. Thostenson, C. Li, T.W. Chou, Review: Nanocomposites in context, Composites Science and Technology 65, (2005), 491-516.

[6] J. He, M. Ice, S. Dallek, and E. J. Lanernia, Synthesis of Nanostructured WC-12 Pct Co Coating Using Mechanical Milling and High Velocity Oxygen Fuel Thermal Spraying, Metallurgical and Materials Transactions A 31A, (2000), 541-553.

[7] J. He, M. Ice, S. Dallek, and E. J. Lanernia, Synthesis of Nanostructured Cr_3C_2-25(Ni20Cr) Coatings, Metallurgical and Materials Transactions A 31A, (2000), 555-564.

[8] Y.C. Kang, S. L. Chan, Tensile properties of nanometric Al_2O_3 particulate- reinforced aluminum matrix composites, Materials Chemistry and Physics 85, (2004), 438-443.

[9] D.Y. Ying and D.L. Zhang, Processing of Cu-Al_2O_3 metal matrix nanocomposite materials by using high energy ball milling, Mater. Sci. Eng. A 286, (2000), 152-156.

[10] M. Kok, Production and Mechanical Properties of Al_2O_3 Particle-Reinforced 2024 Aluminium Alloy Composites, J. Mater. Process. Technol. 161, (2005), 381-387.

[11] Brahim, I.A., Mohamed, F.A. and Lavernia, E.J. Particulate reinforced metal matrix composites-a review, Journal of Materials Science 26, (1991), 1137-1156.

[12] K.U. Kainer, B.L. Mordike, F. Hehmann (Eds.), Magnesium Alloys and Their Applications, DGM Informationsgesellschaft, (1993), Oberursel, Germany, 415-422.

[13] V. Laurent, P. Jarry, G. Regazzoni, D. Apelian, Processing- Microstructure Relationships in Compocast Magnesium/SiC, J. Mater. Sci. 27, (1992), 4447-4459.

[14] R.A. Saravanan, M.K. Surappa, Fabrication and characterisation of pure magnesium-30 vol.% SiC_P particle composite, Mater. Sci. Eng. A 276, (2000), 108-116.

[15] A. Luo, Processing, microstructure, and mechanical behavior of cast magnesium metal matrix composites, Metall. Mater. Trans A 26A, (1995), 2445-2455.

[16] Y. Cai, M.J. Tan, G.J. Shen, H.Q. Su, Microstructure and Heterogeneous Nucleation Phenomena in Cast SiC Particles Reinforced Magnesium Composite, Materials Science and Engineering, Mater. Sci. Eng. A 282, (2000), 232-239.

[17] H. Hu, Grain Microstructure Evolution of Mg (AM50A)/SiCp Metal Matrix Composites, Scripta Mater 39, (1998), 1015-1022.

[18] B.W. Chua, L. Lu, M.O. Lai, Influence of SiC particles on mechanical properties of Mg based composite, Compos. Struct 47, (1999), 595-601.

[19] L. Hu, E. Wang, Fabrication and mechanical properties of SiCW/ ZK51A magnesium matrix composite by two-step squeeze casting, Mater. Sci. Eng. A 278, (2000), 267-271.

[20] M.Y. Zheng, K. Wu, C.K. Yao, Effect of interfacial reaction on mechanical behavior of SiCw/AZ91 magnesium matrix composites, Mater. Sci. Eng. A318, (2001), 50-56.

[21] R.Z. Valiev, R.K. Islamgaliev, I.V. Alexandrov, Bulk nanostructured materials from severe plastic deformation, Progress in Materials Science 45, (2000), 103-189.

[22] He. F, Han. Q. and Jackson,M.J, Nanoparticulate reinforced metal matrix nanocomposites-a review, Int. J. Nanoparticles, Vol.1, No.4, (2008), 301-309.

[23] Luke Fischer, Rishi Raj, Atanu Saha, Literature Suevey Report: Nano- dispersion Strengthening of Aluminum, (2004).

[24] Crainic, N., and Marques, A. T., Nanocomposites: A State-of-Art Review, Key Eng. Mater. 230-232, (2002), 656-659.

[25] Rawal, S., Metal-Matrix Composites for Space Applications, ASME J. Offshore Mech. Arct. Eng. 53, (2001), 14-17.

[26] Varuzan M. Kevorkijan, Aluminum Composites for Automotive Applications: A Global Perspective, JOM 51, (1999), 54-58.

[27] S.W. Hadley, S. Das, J.W. Miller, Aluminum R&D for Automotive Uses And the Department of Energy's Role, (1999), 157.

[28] G.E. Dieter, Mechanical Metallurgy, (1986), McGraw Hill Book Inc, U.S.A.

[29] G.I. Eskin, Principles of Ultrasonic Treatment: Application for Light Alloy Melts, Adv. Perform. Mater. 4, (1997), 223-232.

[30] X. Jian, H. Xu, T.T. Meek, Q. Han, Effect of power ultrasound on solidification of aluminum A356 alloy, Mater. Lett. 59, (2005), 190-193.

[31] V. Abramov, O. Abramov, V. Bulgakov, F. Sommer, Solidification of aluminium alloys under ultrasonic irradiation using water-cooled resonator, Mater. Lett. 37, (1998), 27-34.

[32] X. Jian, T.T. Meek, Q. Han, Refinement of Eutectic Silicon Phase of Aluminum A356 Alloy Using High-Intensity Ultrasonic Vibration, Scripta Mater. 54, (2006), 893-896.

[33] M. Abdel-reihim, W. Reif, Effect of ultrasonic vibrations on the solidifications of alloys containing different microstructures, Metall 38, (1984), 130-133.

[34] Yang Y, Lan J, Li XC. Study on bulk aluminum matrix nano-composite fabricated by ultrasonic dispersion of nano-sized SiC particles in molten aluminum alloy. Mater Sci Eng A, 380, (2004), 373-378.

[35] Razavi Tousi SS, Yazdani Rad R, Salahi E, Mobasherpour I, Razavi M. Production of Al-20 wt.% Al_2O_3 composite powder using high energy milling. Powder Technol., 192, (2009), 346-351.

[36] Habibnejad-Korayem M, Mahmudi R, Ghasemi HM, Poole WJ. Tribological behavior of pure Mg and AZ31 magnesium alloy strengthened by Al_2O_3 nanoparticles. Wear, 268, (2010), 405-412.

[37] Radi Y, Mahmudi R. Effect of Al_2O_3 nano-particles on the microstructural stability of AZ31 Mg alloy after equal channel angular pressing. Mater Sci Eng A, 527, (2010), 2764-2771.

[38] Lu L, Thong KK, Gupta M. Mg-based composite reinforced by Mg_2Si. Compos Sci Technol 63, (2003), 627-632.

[39] Wang HY, Jiang QC, Zhao YQ, Zhao F, Ma BX, Wang Y. Fabrication of TiB2 and TiB2-TiC particulates reinforced magnesium matrix composites. Mater Sci Eng A 372, (2004), 109-114.

[40] Mula S, Padhi P, Panigrahi SC, Pabi SK, Ghosh S. On structure and mechanical properties of ultrasonically cast Al-2% Al_2O_3 nanocomposite. Mater Res Bull, 44, (2009), 1154-1160.

[41] B. Wielage, I. Hoyer, S. Weis, Soldering Aluminum Matrix Composites, Weld. J. 86, No.3, (2007), 67-70.

[42] Z.W. Xu, J.C. Yan, G.H. Wu, X.L. Kong, S.Q. Yang, Interface structure and strength of ultrasonic vibration liquid phase bonded joints of Al_2O_3p/6061Al composites, Scripta Mater. 53, (2005), 835-839.

[43] J.C. Yan, H.B. Xu, Z.W. Xu, L. Ma, S.Q. Yang, Mater. Sci. Technol. 20, (2004), 1-4.

[44] Z. Li, W. Fearis, T.H. North, Particulate Segregation and Mechanical-Properties in Transient Liquid-Phase Bonded Metal-Matrix Composite-Material, Mater. Sci. Technol. 11, (1995), 363-369.

[45] A. Ureña, L. Gil, E. Esciche, J.M. Gómez de Salazar, M.D. Escalera, High temperature soldering of SiC particulate aluminium matrix composites (series 2000) using Zn-Al filler alloys, Sci. Technol. Weld. Join. 6, (2001), 1-11.

[46] J. Hashim, L. Looney, M.S.J. Hashmi, Metal matrix composites: production by the stir casting method, J. Mater. Process. Technol. 92-93, (1999) 1-7.

[47] J.A. Garcia-Hinojosa, R.C. Gonz ález, I.J.A. Ju árez, M.K. Surrapa, Effect of grain refinement treatment on the microstructure of cast Al-7Si-SiCp composites, Mater. Sci. Eng. A386, (2004), 54-60.

[48] Lan J, Yang Y, Li XC. Microstructures and microhardness of SiC nanoparticles reinforced magnesium composites fabricated by ultrasonic method. Mater Sci Eng A 386, (2004), 284-290.

[49] Cao G, Choi H, Konishi H, Kou S, Lakes R, Li X. Mg-6Zn/1.5% SiC nanocomposites fabricated by ultrasonic cavitation-based solidification processing. J Mater Sci. 16, (2008), 5521.

[50] Yan JC, Xu ZW, Shi L, Ma X, Yang SQ. Ultrasonic assisted fabrication of particle reinforced bonds joining aluminum metal matrix composites. Mater Des 2011, (2011), 343-347.

[51] He. F, Han. Q. and Jackson,M.J., Nanoparticulate reinforced metal matrix nanocomposites-a review, Int. J. Nanoparticles 1, (2008), 301- 309.

[52] Guozhong Cao, Nanostructures & nanomaterials: synthesis, properties & applications, Imperial College Press, (2004).

[53] J D Fast, Interaction of Metals and Gases, Academic Press, (1965).

[54] J. Lan, Y. Yang, X Li, Microstructure and microhardness of SiC nanoparticles reinforced magnesium composites fabricated by ultrasonic method, Materials Science and Engineering A 386, (2004), 284-290.

[55] X. LI, Y. Yang, X. Cheng, Ultrasonic-assisted fabrication of metal matrix nanocomposites, Journal of Materials Science 39, (2004) 3211-3212.

[56] Y. Yang, X. Li, Ultrasonic Cavitation-Based Nanomanufacturing of Bulk Aluminum Matrix Nanocomposites, Transactions of the ASME 129, (2007), 73.

[57] Y. Yang, J. Lan, X. Li, Study on bulk aluminum matrix nano-composite fabricated by ultrasonic dispersion of nano-sized SiC particles in molten aluminum alloy, Materials Science and Engineering A 380, (2004), 378-383.

[58] Laurentiu Nastac, Modeling of Casting, Welding and Advanced Solidification Processes XII, Vancouver, June 7-14, (2009), TMS.

[59] Laurentiu Nastac, Yi Dai, Ultrasonic Model Development and Applications to Ingot Casting Processes, (2008), ANSYS conference.

[60] X. Li, R. Lakes, S. Kou, J. Groza, K. Gall, Fundamental Study of Bulk Magnesium Alloy Matrix Nanocomposites Fabricated by Ultrasonic Cavitation Based Solidification Processing, Nanoscale Science and Engineering Grantees Conference, Dec 4-6, (2006).

[61] Pradeep Rohatgi, Rajiv Asthana. The solidification of metal-matrix particulate composites. JOM 43, (1991), 35-41.

[62] Laurentiu Nastac, Mathematical Modeling of the Solidification Structure Evolution in the Presence of Ultrasonic Stirring, Met Trans B, 42B, (2011), 1297-1305.

[63] L. Nastac, Multiscale modeling of the solidification microstructure evolution in the presence of ultrasonic stirring, IOP Conference Series: Materials Science and Engineering, (2012), http://iopscience.iop.org/1757-899X/33/1/012079

[64] L. Nastac, Numerical Modeling of Solidification Morphologies and Segregation Patterns in Cast Dendritic Alloys, Acta Materialia 47, (2011), 4253-4262.

[65] C. E. Brennen, Cavitation and Bubble Dynamics, Oxford University Press, (1995), 51.

[66] L. Nastac, Modeling and Simulation of Microstructure Evolution in Solidifying Alloys, Springer, 2004: http://www.springer.com/materials/special+types/book/978-1-4020-7831-6

[67] J. Hashim, L. Looney, M.S.J. Hashmi, Metal Matrix composites: production by the stir casting method, J. Mater. Process. Technol. 92-93, (1999), 1-7.

[68] J.A. Garcia-Hinojosa, R.C. Gonz âlez, I.J.A. Ju árez, M.K. Surrapa, Effect of grain refinement treatment on the microstructure of cast Al-7Si-SiCp composites, Mater. Sci. Eng. A386, (2004), 54-60.

[69] X Li, Y. Yang, D. Weiss, Theoretical and experimental study on ultrasonic dispersion of nanoparticles for strengthening cast Aluminum Alloy A356, Metallurgical Science and Technology 26-2, (2008).

[70] Su B, Yan HG, Chen G, Shi JL, Chen JH, Zeng PL. Study on the preparation of the SiCp/Al-20Si-3Cu functionally graded material using spray deposition. Mater Sci Eng A (2010); 527:6660.

[71] Seyed Reihani SM.Processing of squeeze cast Al 6061-30 vol% SiC composites and their characterization. Mater Des (2006); 27:216-222.

[72] Bozic D, Dimcic B, Dimcic O, Stasic J, Rajkovic V. Influence of SiC particles distribution on mechanical properties and fracture of DRA alloys. Mater Des (2010);31:134-141.

[73] Michael P, De Cicco, Li XC, Lih-Sheng Turng. Semi-solid casting (SSC) of zinc alloy nanocomposites. J Mater Proc Technol (2009);209:5881.

[74] G.I. Eskin, Principles of Ultrasonic Treatment: Application for Light Alloy Melts, Adv. Perform. Mater. 4, (1997), 223-232.

[75] X. Jian, H. Xu, T.T. Meek, Q. Han, Effect of power ultrasound on solidification of aluminum A356 alloy, Mater. Lett. 59, (2005), 190-193.

[76] K. Akio, O. Atsushi, K. Toshiro, T. Hiroyuki, J. Jpn, Fabrication, process of metal matrix composite with nano-size SiC particle produced by vortex method, Inst. Light Met. 49, (1999), 149-154.

[77] K.M. Mussert, W.P. Vellinga, A. Bakker, S. Van Der Zwaag, A nano-indentation study on themechanical behavior of the matrix material in an AA6061-Al_2O_3 MMC, J. Mater. Sci. 37, (2002), 789-794.

[78] X.F. Chen, E.G. Baburai, F.H. Froes, A. Vassel, Ti-6Al-4V/SiC composites by mechanical alloying and hot isostatic pressing, Proc. Adv. Part. Mater. Processes, (1997), 185-192.

[79] S.L. Urtiga Filho, R. Rodriguez, J.C. Earthman, E.J. Lavernia, Synthesis of diamond reinforced Al-Mg nanocrystalline composite powder using ball milling, Mater. Sci. Forum 416-418, (2003), 213-218.

[80] J.R. Groza, Sintering of nanocrystalline powders, Int. J. Powder Metall. 35, (1999), 59-66.